Orbital
The electronic journal of chemistry

the electronic journal of chemistry

Review | http://dx.doi.org/10.17807/orbital.v17i4.23400

Titanium Dioxide (TiO_2) and Photocatalysis: A Detailed Overview of the Synthesis, Applications, Challenges, Advances and Prospects for Sustainable Development

Yago K. S. França* [a], Kauê S. Pereira [a], Yasmin H. C. Feitosa [a], Vitor B. Marques [a], and Danilo R. Souza* [a]

Emerging contaminants in aquatic ecosystems demand advanced remediation strategies, with semiconductor photocatalysis standing out as a transformative technology. This review examines material design innovations, focusing on sol-gel, hydrothermal, and ultrasonic synthesis methods that enable precise control over structural properties critical for photocatalytic efficiency. Doping with metals/non-metals and heterostructure engineering are highlighted for adjusting bandgap energy to enhance visible-light absorption. Advanced characterization techniques, including XRD and electron microscopy, reveal correlations between material architecture and performance. Applications encompass solar-driven degradation of pharmaceuticals, antimicrobial surface coatings, and hybrid systems combining photocatalysis with membrane filtration or ozonation. Scalability challenges are addressed through immobilized catalysts and reactor design innovations. Interdisciplinary approaches integrating AI optimization and agro-industrial waste valorization underscore sustainable synthesis pathways. Functionalized materials demonstrate dual utility in environmental and biomedical contexts, while solar hydrogen production aligns with clean energy objectives. Persistent barriers include energy efficiency optimization and long-term catalyst stability. Future research emphasizes adaptive material architectures, circular economy integration, and synergistic coupling with conventional treatment processes. By bridging lab-scale advances with industrial scalability, photocatalysis emerges as a versatile solution for water purification and sustainable resource management, offering a roadmap for addressing complex environmental challenges.

Graphical abstract

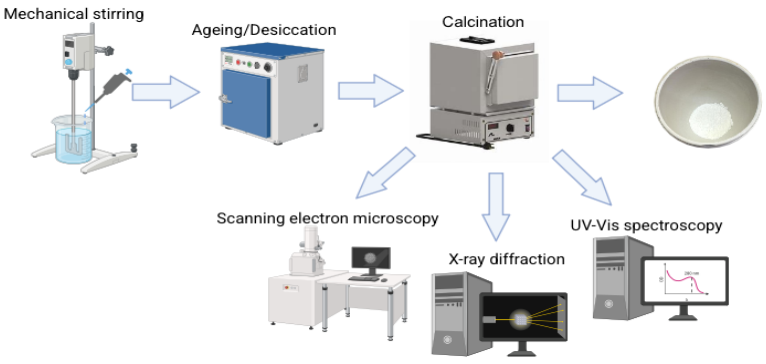

Keywords

Doping strategies
Emerging contaminant
Green synthesis
Semiconductor photocatalysis
Solar driven
TiO_2 synthesis

Article history

Received 12 May 2025
Revised 26 Jul 2025
Accepted 31 Jul 2025
Available online 19 Aug 2025

Handling Editor: Adilson Beatriz

1. Introduction

[a] Center for Exact Sciences and Technologies - Federal University Western of Bahia; Barreiras, Ba, Brazil. *Corresponding author. E-mail: **yago.franca@ufob.edu.br; danilo.souza@ufob.edu.br**

Environmental contamination is one of the most serious contemporary challenges, exerting substantial influences on both ecological integrity and human well-being. Globally notorious pollutants such as plastics, heavy metals and pesticide compounds have been the focus of intense environmental concern over the years. The origin of these pollutants is often linked to industrial processes, agricultural practices and urban dynamics, and their environmental persistence can lead to bioaccumulation in food chains, which can directly and indirectly result in adverse effects on human health [1]. Some pollutants that are less known to the general population are referred to as emerging contaminants. Emerging contaminants constitute a growing challenge for environmental quality and public health. The increase in the production and use of various chemical substances, such as pharmaceuticals and pesticides, has resulted in the discharge of complex compounds that are difficult to remove from aquatic environments [2]. The complexity of these substances, combined with the inefficiency of conventional sewage treatment systems in removing them, aggravates the situation, since many emerging contaminants are persistent in the environment, accumulating over time and contaminating the food chain [3].

Given the growing concern about the presence of emerging contaminants in water resources, the search for effective treatment technologies is intensifying. Photocatalysis stands out as a promising alternative in this context, since it promotes the degradation of a wide variety of complex organic compounds through the generation of powerful oxidants, such as the hydroxyl radical [4]. High efficiency, versatility and the production of less toxic by-products are characteristics that make photocatalysis attractive for water decontamination. However, large-scale application still faces challenges related to process optimization, operating costs and the generation of inorganic by-products [5].

2. Emerging contaminants

Emerging contaminants are synthetic or natural chemical substances, produced on a large scale and released into the environment, often found in nature in low concentrations, but with significant potential to cause damage to human health and ecosystems. Examples include pharmaceuticals, pesticides, personal care products, hormones and microplastics [6]. These substances, also referred to as contaminants of emerging concern (CECs), encompass a diverse array of chemical and biological agents whose risks are not fully understood and are not yet regulated under conventional environmental policies. Their occurrence results from anthropogenic activities and they may undergo long-range transport, transformation, and bioaccumulation, contributing to complex environmental mixtures with unpredictable effects [7]. Due to the delay in understanding the impact of these substances, justified by the increase in the number of publications in recent years (Fig. 1) and the complexity of their chemical structures, these contaminants are not adequately covered by traditional environmental legislation, making their monitoring and control more challenging [8].

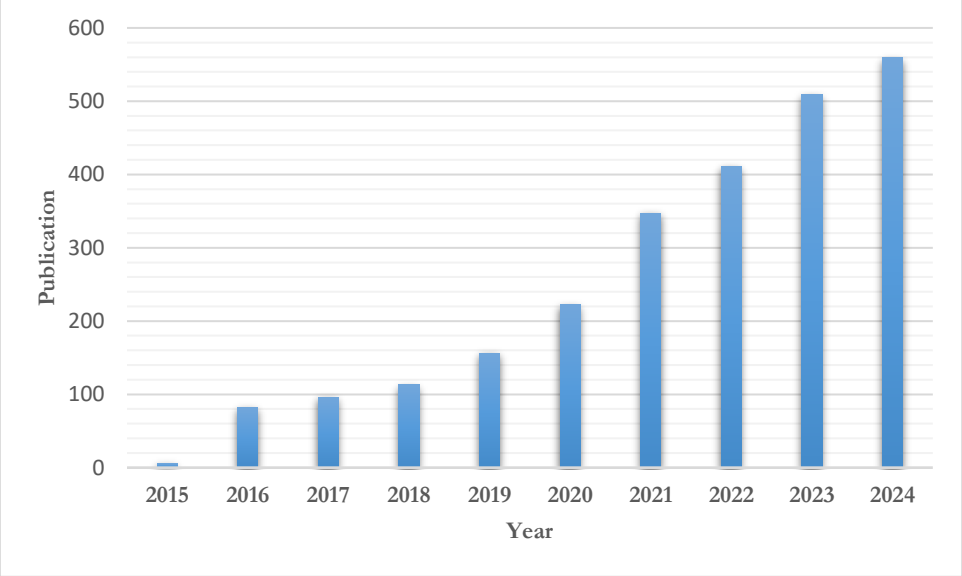

Fig. 1. Number of publications on emerging contaminants during the period 2014 to october 2024 [9].

The presence of emerging contaminants in water resources can cause a series of environmental and public health problems. These compounds can disrupt the balance of aquatic ecosystems, affect the reproduction and development of aquatic organisms, and bioaccumulate in the food chain, ultimately reaching humans [10]. Furthermore, studies indicate that some emerging contaminants may be associated with the emergence of antimicrobial resistance, hormone disruption and other chronic effects on human health [11]. Conventional sewage treatment plants (STPs) are not designed to efficiently remove emerging contaminants [12]. Many of these substances are resistant to biological and physical-chemical treatment processes, passing through sewage treatment plants and reaching the receiving water bodies [13]. The complexity of the matrix of emerging contaminants, with a great diversity of substances and their combinations, further complicates the development of effective technologies for their removal [14].

Emerging contaminants are highly persistent in the environment and can remain for long periods in soils,

sediments and water [4]. Bioaccumulation of these compounds in the food chain represents a significant risk to human health and biodiversity. This risk is intensified by the lack of adequate instruments in the environmental legislation of many countries to regulate the presence of these contaminants in the environment. The absence of specific regulations and maximum permitted limit's hinders the control and management of these pollutants [8]. Given the challenges posed by emerging contaminants, various treatment alternatives have been investigated. Advanced oxidation processes, adsorption on activated carbon, membranes and biofilms are some of the promising technologies for removing these compounds [15–17]. In addition, preventing contamination by reducing the production and improper disposal of these products is fundamental to minimizing environmental impacts. The implementation of different technologies and the adoption of sustainable practices are crucial to addressing this global challenge.

3. Photocatalysis

The growing concern about the presence of emerging contaminants (ECs) in water resources has driven the search for efficient and sustainable treatment technologies. In this context, heterogeneous photocatalysis (HPC) is emerging as a promising alternative for the degradation of a wide range of recalcitrant organic substances [4].

HPC is based on the ability of semiconductor materials, such as titanium dioxide (TiO_2), to absorb light energy and generate electron-hole pairs. When these pairs interact with water and oxygen molecules present in the aqueous medium, they induce the formation of reactive oxygen species (ROS), mainly hydroxyl radicals (●OH). Due to their high reactivity, ●OH radicals are able to oxidize and mineralize ECs, generating by-products more amenable to mineralization, with reduced biorecalcitrance and enhanced biodegradability [18]. The scheme for producing ROS in TiO_2 nanoparticles is shown in Fig. 2.

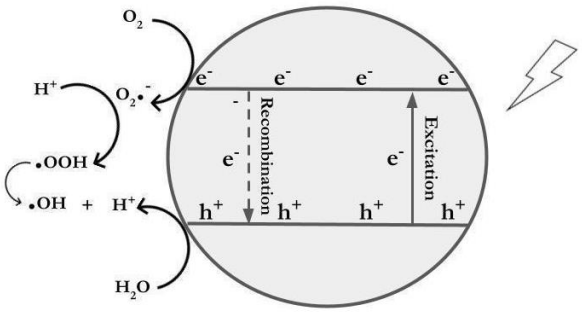

Fig. 2. Scheme of activation of TiO_2 nanoparticles under light incidence for generation of oxidative species (Modified by author) [19].

The efficiency of HPC is influenced by several factors, such as the nature of the photocatalyst, the intensity and wavelength of the incident radiation, the concentration of contaminants, the pH of the solution and the presence of other ions and organic compounds [20]. HPC has significant advantages over other treatment processes, including the possibility of using sunlight as an energy source, the non-generation of toxic by-products and high efficiency in degrading a wide variety of organic compounds. However, some limitations still need to be overcome, such as the low photocatalytic activity in alkaline pH conditions and the difficulty in removing the photocatalyst from the aqueous medium after treatment [21].

The applications of photocatalysis are not limited to the degradation of pollutants in aqueous media. The production of supercapacitors represents a promising alternative for improving electronic devices and energy storage systems. Moreover, photocatalysis can improve the efficiency of capturing energy from renewable sources using photocatalytic oxides [22].

Photocatalysis can be applied in combination with membrane technology for the sustainable and continuous purification of wastewater. This integrated approach takes advantage of both technologies, where photocatalysis degrades hard-to-remove organic pollutants and membrane separation filters out particles and contaminants. The combination results in a more efficient and far-reaching purification process, reducing the need for additional energy and increasing the durability of the membranes by preventing the build-up of dirt [23].

Photocatalysis can also be applied to the generation of green hydrogen through water splitting. Nanocomposites demonstrate significantly higher photocatalytic efficiency than pure materials, with a significantly higher hydrogen generation rate. Hierarchical porous structures provide efficient channels for charge transport, improving the separation and migration of photoinduced charge carriers, which results in greater efficiency in hydrogen generation [24].

4. TiO_2

TiO_2 is a semiconductor ceramic material that has three crystalline phases: brookite, anatase and rutile. The brookite phase is metastable and tends to convert into more stable phases, as anatase and rutile, especially under heating. The transition from brookite to anatase occurs around 400°C, while anatase converts irreversibly to rutile when subjected to higher temperatures. These transformations are crucial for scientific applications, as the anatase and rutile phases are more stable and therefore more common in studies [25]. TiO_2 is notable for its potential in photocatalytic processes, although its efficacy is limited by factors such as its narrow electromagnetic absorption spectrum and bandgap energy located in the ultraviolet region. The rutile phase has a bandgap energy of approximately 3.02 eV, while anatase has around 3.20 eV. The anatase phase, despite having a slightly higher bandgap energy, offers a larger surface area, which results in a greater availability of active sites for adsorption and, consequently, a better photocatalytic performance [26].

To optimize the photocatalytic activity of TiO_2, a higher proportion of anatase relative to rutile is desirable. Achieving a structural configuration with predominant anatase content can be accomplished by controlling synthesis parameters, including thermal treatment and the molar ratio of precursors used in the synthesis method [27].

To overcome the current limitations of photocatalyst materials as TiO2, researchers have been working on innovative methods, among which the doping of materials stands out as a promising method. This technique involves the deliberate incorporation of impurity atoms into the crystal lattice, altering the intrinsic electronic properties of the

materials with the purpose of enhancing their photocatalytic efficacy. The addition of transition metals, such as iron, silver and copper, and non-metallic elements, such as carbon, nitrogen and sulphur, has revealed vast potential by inducing intermediate electronic states that allow light to be captured in the visible spectrum, thus increasing the material's photocatalytic capacity. Doping can be carried out alone or in combination, aiming for synergies that maximize the desired characteristics [28,29].

In addition to TiO_2, other semiconductors can be used for the same purpose, such as ZnO, which exhibits similar properties and low cost; CdS, which is active under visible light despite its toxicity; and WO_3, known for its stability and visible-light responsiveness [30,31,32].

5. Synthesis methods

5.1 Sol-gel

The sol-gel method is a synthesis technique that is renowned for its flexibility and wide applicability in the production of materials. This process involves the transformation of a colloidal solution (sol) into a solid three-dimensional network (gel), allowing the creation of a wide range of materials, including semiconductor oxides and aerogels, which find diverse technological applications. Precise adjustment of the synthesis conditions, such as temperature, pH and precursor concentration, allows materials with different physical and chemical properties to be obtained [31].

One of the primary uses of the sol-gel method is the production of thin metal oxide films, which are crucial for applications in electronics and photonics. In these fields, uniformity and control of film thickness are essential for device performance. Furthermore, the technique allows for the creation of hybrid materials that combine organic and inorganic properties, resulting in materials with innovative functionalities and potential for various technological applications [32]. The sol-gel method is also prominent in the manufacture of biochemical sensors and detection materials. The incorporation of enzymes into the gel matrix makes it possible to develop highly sensitive and specific sensors suitable for a wide range of bioanalytical applications [19,33–35].

The sol-gel method has proven to be a highly effective approach for the synthesis of photocatalytic semiconductor materials, which are crucial for applications in pollutant decomposition and clean energy production. This method allows precise control of the morphology, structure and composition of the photocatalysts, resulting in materials with high efficiency in absorbing light and promoting photocatalytic reactions. By adjusting the synthesis conditions, such as temperature, pH and precursor concentration, it is possible to develop materials with optimized properties for using sunlight to produce energy, making this method a powerful tool in the search for sustainable solutions to environmental and energy problems [30].

The synthesis of semiconductor materials via the sol-gel method begins with the dissolution of metal precursors, such as alkoxides, in polar solvents, under controlled pH and temperature conditions, to form a homogeneous sol. At this stage, sequential hydrolysis and condensation reactions govern the formation of the microstructure: hydrolysis replaces alkoxide groups (OR) with hydroxyls (●OH), generating reactive intermediates (M-OH), while condensation promotes the formation of covalent bonds (M-O-M) via dehydration, establishing a three-dimensional polymeric network [36]. Nucleation and growth of colloidal particles are modulated by intermolecular forces, culminating in system percolation and sol-gel transition. Gelation, accompanied by syneresis, consolidates the porous matrix through cross-linking, while aging optimizes structural cohesion via Ostwald ripening and thermodynamic rearrangement [37].

Afterwards, the wet gel undergoes controlled drying to remove residual solvents, minimizing capillary tensions that induce cracks Kinetics of Supercritical Drying of Gels [38]. The resulting xerogel is calcined (300 - 800 °C) to degrade organic substances and induce crystallization. Parameters such as heating rate and isotherm time regulate the nucleation of crystalline phases, crystallite size and defect density Effect of Calcination Temperature on Photocatalytic Activity of Synthesized TiO2 Nanoparticles via Wet Ball Milling Sol-Gel Method [39]. Photocatalytic efficiency is maximized by the balance between high surface area, porosity and surface-accessible active sites, properties that are intrinsically dependent on the synthetic conditions at each stage. This precise control enables the quantum reactivity and mechanical stability of the final material to be optimized. The synthetic route of TiO_2 is elucidated in figure 3.

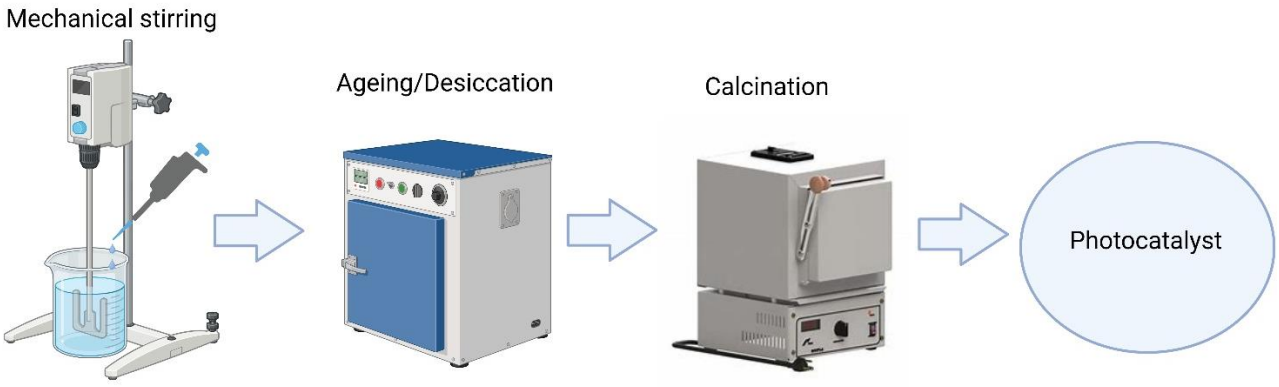

Fig. 3. Synthetic route of photocatalyst nanomaterials by the sol-gel method.

One of the main advantages of the sol-gel method is the precise control over the morphology and structure of

semiconductor oxides, which directly influences their properties. This ability to adjust allows the production of materials with specific characteristics that meet the requirements of different technological applications. In addition, the method stands out for being more cost-effective compared to conventional synthesis techniques, allowing the manufacture of a wide range of materials with diverse compositions and structures [40]. However, the sol-gel method is not without its drawbacks. One of the challenges faced is ensuring the homogeneity of the final product, especially when applied on larger scales. Additionally, the processing time can be prolonged due to the steps required for drying and calcination. Another critical aspect is contamination, impurities present in the precursors can negatively affect the properties of the final material [41]. Despite these limitations, the advantages of the sol-gel method in the synthesis of semiconductor oxides continue to drive its use in research and industrial applications, highlighting its fundamental role in technological innovation [42].

The analysis of the data presented in Table 1 reveals a significant diversity of approaches in the sol-gel synthesis of TiO_2, such as the non-hydrolytic route, which is the replacement of the traditional hydrolysis process with alkanolysis, where alcohol acts as the only solvent in the absence of water [43]. The non-hydrolytic route represents an interesting alternative for the morphological control of TiO_2, as the absence of water eliminates the competition between hydrolysis and condensation, allowing better control over particle growth and their final structural characteristics [44].

Table 1. Sol-gel synthesized photocatalysts: comparative experimental conditions and degradation efficiency for emerging contaminants.

Photocatalyst	Contaminants	Synthesis conditions	Photodegradation conditions	References
TiO_2 anatase	Tetracycline	H_2O:ROH (1:10) molar proportion 300 rpm stirring Calcination temperature 400 °C - 800 °C	100 % 20 min, UV	[45]
TiO_2 anatase	Paracetamol	Non-hidrolitic rout Stirring for 10 h at 150 °C	38,47 % 120 min, VIS	[46]
Ct-TiO_2	Bisphenol	Stirring for 24 h at 90 °C Washed the precipitate	99 % 240 min, VIS	[47, 48]
AC/TiO_2	Estradiol	$TiCl_4$ (Precursor Ti) Dried at 100 ◦C overnight.	100 % 60 min, VIS	[49]
TiO_2	Bentazon	Stirring in ice bath Dried at 80 °C for 18 h	99 % 70 min, UV	[50]
ZnO	Methylene blue	1 h stirring at 70 °C *Lidah Mertua* Extract separate the precipitate	90 % 120 min, UV	[51]
ZnO	Methylene blue	4 h stirring at 60 °C Bacteria and crustaceans powder Separate the precipitate	60 % 60 min, UV	[52]
Zn-$AlPO_4$	Fipronil	Non-Hydrolytic Refluxed at 110 °C for 4 h Aged overnight	80 % 120 min, UV	[43]
SiO_2	Methyl orange	Rice husk ash (Si source) 4 h stirring at room temp. 48 h aged	95 % 150 min, UV	[53]
La_2Ti2O7	Rhodamine B	30 min stirring Glycine-assisted Aged at 80 °C overnight	100 % 90 min, UV	[54]

The deployment of natural extracts (e.g., Lidah Mertua [51]) and bacterial/crustacean biomass [52] in sol-gel photocatalyst synthesis delivers multidimensional advantages transcending conventional environmental impact mitigation. These bioresources function as multifunctional platforms, wherein bioactive constituents (polyphenols, terpenoids, and proteins) operate synergistically as: (i) reducing agents, (ii) colloidal stabilizers, and (iii) natural dopant sources - collectively enhancing the optoelectronic characteristics of resultant materials [53]. A particularly noteworthy attribute is their precise modulation of nanoparticle morphology and size distribution during gelation, yielding tailored surface area (BET >150 m^2g^{-1}) and hierarchical porosity (2-50 nm range), both critical for photocatalytic quantum efficiency [55].

Furthermore, the upcycling of agroindustrial waste (e.g., rice husk-derived mesoporous SiO_2 [53],) establishes a technological symbiosis between circular economy paradigms and advanced material engineering, achieving 40-60% reduction in both production costs and cradle-to-gate energy intensity. Benchmark studies confirm these bio-mediated protocols produce photocatalysts with superior visible-light quantum yields (Φ 420nm ≥ 0.32 vs. 0.18 for conventional counterparts) for emerging contaminant degradation, while demonstrating exceptional operational stability (>30 cycles) [56,57]. This bioinspired synthesis paradigm effectively reconciles sustainability mandates with performance enhancement through molecular-level structure-property control [58].

The combination of different synthesis techniques, the use of an ultrasonic bath and hydrothermal treatment [59], demonstrates a synergy that can optimize the photocatalytic properties of photocatalysts. This integration of methods suggests that the joint application of different techniques can result in a significant improvement in the efficiency and functionality of photocatalytic materials.

Additionally, the use of glycine as an assistant agent in the synthesis proved to be particularly effective, achieving 100% degradation of Rhodamine B in 90 minutes [54], indicating that glycine-assisted self-combustion can promote the formation of crystalline structures with superior photocatalytic activity.

5.2 Hydrothermal

The hydrothermal method enables precise control over material properties (morphology, crystallinity, and particle size) through modulated reaction conditions (temperature, pressure, time), making it indispensable for designing functional nanomaterials [60]. A key application lies in photocatalysis, where its ability to tailor bandgap energies and surface defects enhances light-driven processes such as pollutant degradation and H_2 production [61]. Similarly, in electronics, hydrothermally synthesized oxides (e.g., ZnO, TiO_2) achieve the stoichiometric precision required for high-performance transistors and diodes [62]. This synergy between atomic-level control and scalable processing addresses critical challenges in energy and miniaturization technologies [62].

The hydrothermal method is characterized by the dissolution of precursor substances in water and the application of high temperatures (usually between 100 °C and 300 °C) and pressures. These conditions favor the solubility of the precursors and promote reactions that lead to the formation of new compounds. The reaction occurs in an aqueous solution or with an organic solvent that may contain salts, acids or bases [63]. When heated, these substances ionize, resulting in a supersaturated solution, crucial for the processes of nucleation and crystal growth. The initial dissolution of the precursors results in a mixture where the ions or molecules are free to move, increasing the concentration of the reactive components and, consequently, the probability of new phases forming. The nucleation process is one of the central aspects of the hydrothermal method. As the temperature rises, the concentration of precursors can reach a critical point of supersaturation, leading to the formation of small cores. Nucleation can be homogeneous, occurring without the influence of impurities, or heterogeneous, initiated by surfaces or impurities present in the solution. Once formed, these nuclei become growth centers where atoms or molecules aggregate, occurring by adsorption and diffusion, stabilizing the desired crystalline structure [64].

In general, the synthesis of nanostructured oxides using the hydrothermal method involves steps such as washing the precipitate obtained, followed by drying and finally calcination. Although some materials synthesized by this method do not go through the calcination stage, as the material obtained already has an acceptable level of crystallinity [65]. The general synthetic route of the hydrothermal method is shown in figure 4.

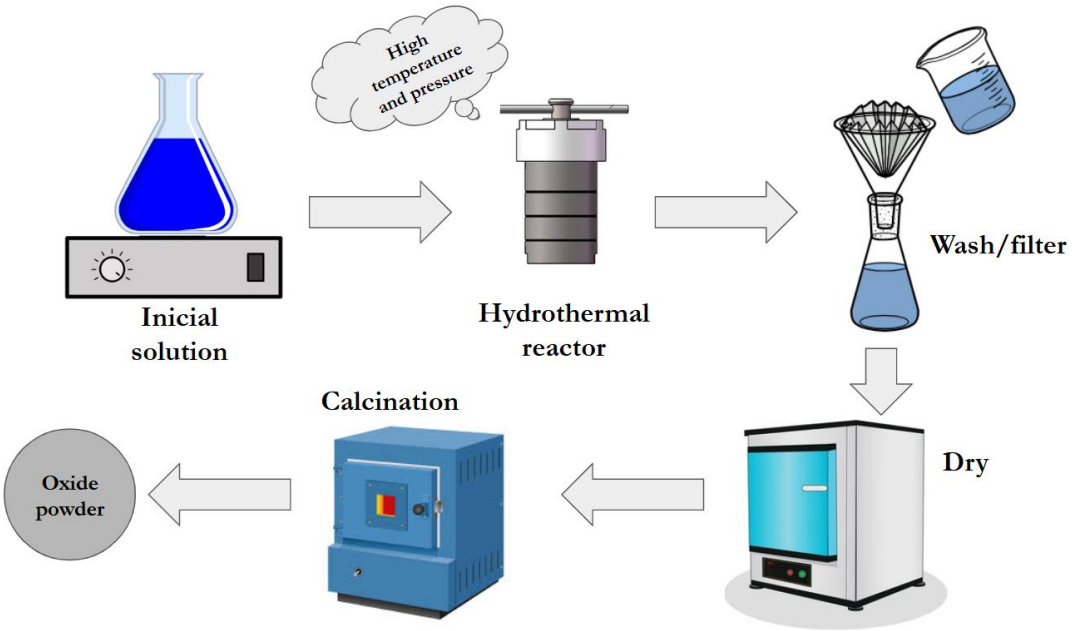

Fig. 4. Synthesis process of nanostructured oxides by the hydrothermal method.

The hydrothermal method is widely recognized for its significant advantages in material synthesis, making it a preferred technique for various scientific and industrial applications. One of its main advantages is the precise control over synthesis conditions, allowing for the modulation of key material properties such as particle size, morphology, and crystallinity [66]. This tunability is essential for meeting the specific requirements of different applications, particularly in nanomaterial production. Moreover, the method operates at relatively low temperatures (typically <200°C) when compared to alternative processes requiring up to 900°C, reducing energy consumption by 40-60% and significantly decreasing the carbon footprint of synthesis while maintaining comparable product quality [67].

Another notable advantage of the hydrothermal method is its simplicity, as it often requires fewer steps than traditional methods such as calcination. This reduction in processing steps not only enhances efficiency but can also shorten the total synthesis time and lower operational costs. These benefits make the method particularly attractive to researchers and industries seeking to develop new materials efficiently [68].

However, the hydrothermal method is not without its drawbacks. One of the main challenges is the high cost of the required equipment, as autoclaves designed to operate under high pressure and temperature conditions tend to be expensive. Additionally, the limited production scale is a significant limitation, as the yield may be restricted, posing challenges to the economic feasibility of large-scale applications. This factor can hinder the broader adoption of the technique in industries that require high material volumes [62].

The complexity of operating the hydrothermal method is also a disadvantage. The high-pressure conditions require special care and strict safety protocols, which may increase operating costs and the need for specialized training. Thus, while the hydrothermal method offers considerable advantages in terms of control and energy efficiency, its limitations in terms of cost, scale of production and operational complexity must be carefully considered when assessing its applicability in industrial and research contexts [69].

Although widely used, conventional heating has intrinsic limitations, such as long reaction times and challenges in precisely controlling the temperature and pressure variables, factors that can compromise the homogeneity and purity of the final product [62]. A compilation of photocatalytic materials synthesized via the hydrothermal method, highlighting these crucial parameters in the context of conventional heating in a muffle furnace, is shown in Table 2.

Table 2. Hydrothermally synthesized photocatalysts: comparative experimental conditions and degradation efficiency for emerging contaminants

Photocatalyst	Contaminants	Synthesis conditions	Photodegradation conditions	References
Co-S-TiO_2	Methylene blue	120 °C 8 h	93 % 120 min, UV – Vis lamp	[70]
BiOBr	Methyl orange	120 °C 6 h	100 % 300 min, Vis	[71]
TiO_2 anatase	Methylene blue	160 °C 5 h Base catalysis	96 % 180 min, Vis	[72]
In_2O_3/RGO	Methylene blue	160 °C 1 h Microwave-assisted	90 % 120 min, UV	[73]
TiO_2 anatase	Ciprofloxacin	180 °C 3 h Microwave assisted	95 % 90 min, Sunlight	[74]
Y-TiO_2	Carbamazepine	200 °C 15 min Microwave-assisted	95 % 240 min, UV	[75]
S-VO_2-Cellulose	Methylene blue	180 °C 24 h	100 55 min, UV	[76]
$BiFeO_3$	Rhodamine B	160 °C 24 h	77 % 45 min, Sunlight	[77]
$LaFeO_3$	Malachite green	200 °C 14 h	80 % 80 min, Sunlight.	[78]

Conversely, microwave-assisted hydrothermal synthesis emerges as an innovative approach to obtaining TiO_2. This technique uses microwave radiation to promote rapid and uniform heating of the reaction medium, resulting in accelerated nucleation processes. Among its main advantages are the significant reduction in reaction time and homogeneous thermal distribution, characteristics that enhance efficiency in the synthesis of materials with improved photocatalytic properties [67].

On the other hand, microwave-assisted hydrothermal synthesis has emerged as a highly effective and innovative strategy for the production of photocatalytic TiO_2-based materials. Unlike conventional methods, this technique enables volumetric and selective heating of the reaction medium through the interaction of microwave radiation with polar solvent molecules, promoting uniform temperature distribution and rapid thermal transfer. These conditions foster instantaneous nucleation and controlled crystal growth, typically resulting in smaller nanoparticles with narrower size distributions [79]. Moreover, microwave irradiation significantly influences the morphological features of the resulting materials, often leading to the formation of structures with high specific surface area, well-defined geometries, and enhanced exposure of catalytically active crystal facets—attributes that are particularly desirable in photocatalysis [73,75,80,81]. In addition to its morphological and structural benefits, this technique is also recognized for its high energy efficiency. Reaction times are drastically reduced—from several hours to just minutes—while minimizing overall energy consumption due to the absence of thermal gradients and the direct conversion of electromagnetic energy into heat. Thus, microwave-assisted synthesis not only accelerates TiO_2 production but also yields materials with superior physicochemical properties, positioning this method as a sustainable and scalable alternative for industrial applications [82].

5.3. Ultrasonic method

Sonochemical synthesis methods are fundamentally based on the phenomenon of acoustic cavitation, a process extensively studied in the field of ultrasound chemistry and comprehensively studied [83]. Cavitation occurs when ultrasonic waves (>20 kHz) propagate through a liquid medium, inducing the formation, growth, and violent collapse of microbubbles. This collapse generates extreme localized conditions—with transient temperatures exceeding 5000 K and pressures above 1000 atm—creating a highly energetic microenvironment that enhances chemical reactions, accelerates nucleation processes, and enables the formation

of products that are often inaccessible via conventional methods [84]. Additionally, acoustic cavitation increases the interfacial area between reactants, resulting in higher yields and improved selectivity in chemical transformations [85]. Another relevant phenomenon in ultrasonic-assisted synthesis is nebulization, which occurs when ultrasound transforms a liquid into a fine mist composed of microdroplets. This technique is particularly advantageous in processes such as ultrasonic spray pyrolysis, in which chemical reactions take place within individual droplets suspended in a gaseous phase, enabling greater morphological control over the resulting particles [86].

Ultrasonic synthesis stands out as a powerful and versatile tool for producing metal oxides with controlled properties and morphologies. The phenomenon of acoustic cavitation, central to this process, generates extreme conditions of temperature and pressure in the bubbles that collapse. This collapse promotes the nucleation and rapid, efficient growth of oxide nanoparticles. Scientific literature documents the successful synthesis of various oxides through the ultrasonication of aqueous solutions of metal salts, highlighting the broad applicability of this technique [86].

Oxide nanoparticles synthesized using ultrasonication have great potential for various applications. A notable example is porous TiO2 microspheres, which stand out for their low cytotoxicity and ability to carry molecules. These characteristics make them promising as targeted drug delivery systems. The ability to target drugs to specific cell compartments opens up new perspectives for the development of more effective treatments for diseases [87].

Ultrasonic methods offer versatility and precise control over the synthesis process. It is possible to manipulate several reaction parameters, such as time, energy input and pressure, allowing the size, morphology and structure of nanomaterials to be customized. Although there are challenges related to energy efficiency in using ultrasound for chemically useful cavitation events, advances in understanding the physics of cavitation promise to make synthesis methods even more effective and efficient in the future. Also, the technology is evolving to overcome difficulties related to scalability, becoming a promising tool for large-scale production of nanostructured materials [88].

The ultrasonic synthesis method for photocatalyst nanomaterials (Fig. 5) is a systematic process that begins with the preparation of two different solutions: one containing metal ions and the other with a precipitating agent, which are then combined and subjected to ultrasonic irradiation using a specific probe [89]. During this process, the phenomenon of acoustic cavitation occurs due to the high-frequency waves generating localized extreme conditions of temperature and pressure, thus facilitating the nucleation and controlled growth of the nanoparticles. The procedure, which can last from minutes to a few hours depending on the desired material [86,90], is completed with separation steps by centrifugation, washing with deionized water and appropriate solvents to eliminate impurities, culminating in oven drying and calcination to obtain the final material.

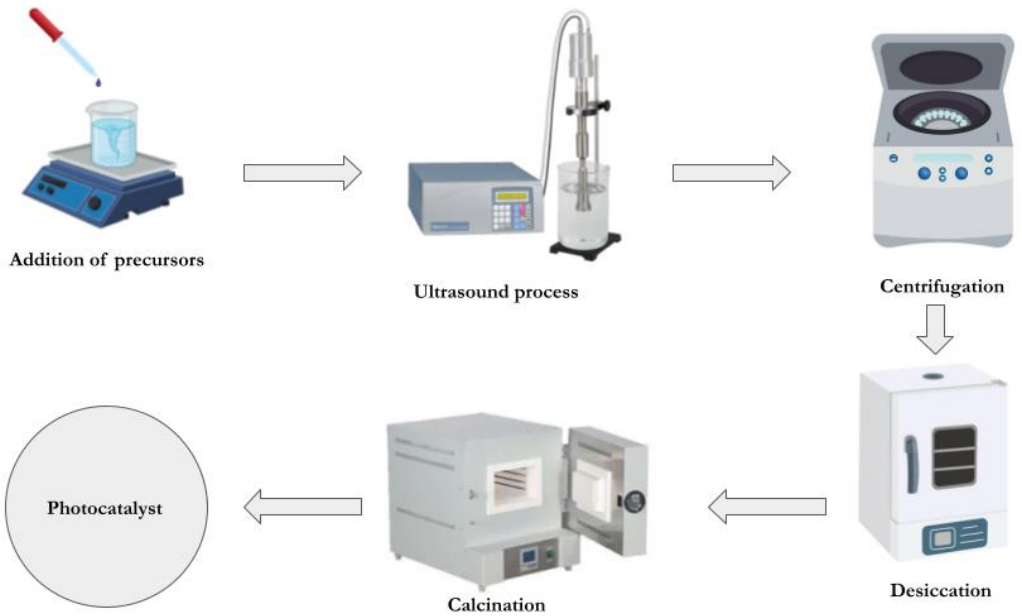

Fig. 5. Photocatalyst synthesis process by ultrasonic method.

Sonochemical synthesis is an innovative technique that uses high-intensity ultrasound to induce chemical reactions in solutions. The process begins with acoustic cavitation, in which sound waves create alternating regions of high and low pressure in a liquid. During the low pressure phase, small gas bubbles form in the solution. These bubbles grow to a critical point and then collapse rapidly during the high pressure phase (Fig. 6). This phenomenon is fundamental for generating extreme conditions that facilitate chemical reactions that would not occur under normal conditions [91].

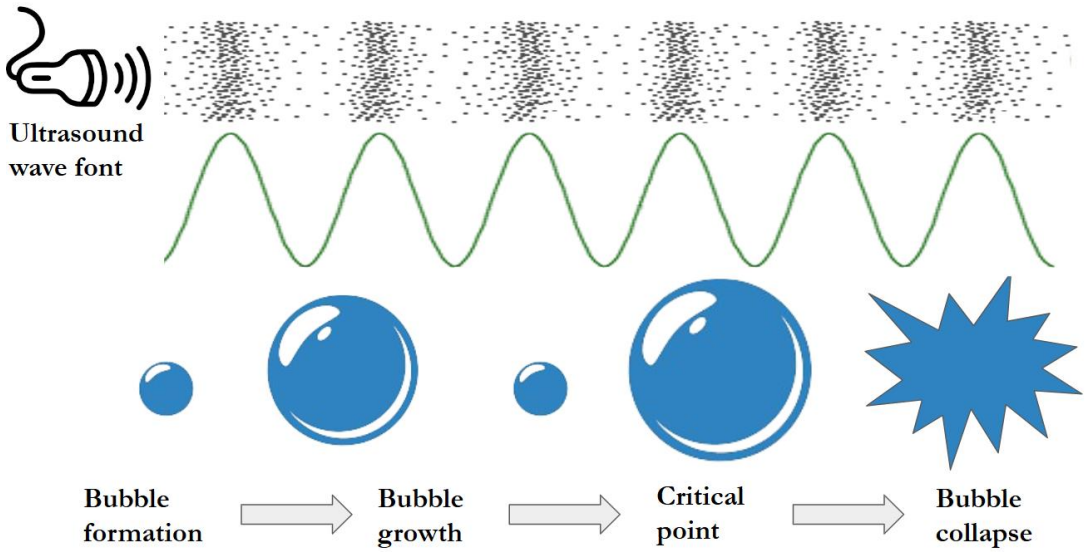

Fig. 6. Illustration of the acoustic cavitation process promoted by ultrasonic adapted from author [92].

The collapse of cavitation bubbles is a crucial event that generates extremely high temperatures, which can exceed 5000 K, and pressures that reach up to 1000 atm, albeit on a very small scale. These extreme conditions create a highly energetic environment, propitious for inducing chemical reactions. The impact of bubble collapse results in an intense release of energy, capable of breaking chemical bonds and promoting the formation of new compounds [93].

One of the most significant effects of bubble collapse is the generation of free radicals, such as hydroxyl (●OH) and hydrogen (●H) radicals. These radicals are highly reactive and play a fundamental role in subsequent chemical reactions, acting as reducing or oxidizing agents, depending on the context of the reaction. The presence of these free radicals is essential for the synthesis of various materials, including metallic nanoparticles [94].

Table 3. Sonochemically synthesized photocatalysts: process optimization and degradation performance for emerging contaminants

Photocatalyst	Contaminants	Synthesis conditions	Photodegradation conditions	References
TiO_2/WO_3	Methylene blue	150 W 5 sec On / 2 sec Off pulses 1 h 25 °C	81 % 180 min	[95]
Ce-TiO_2	Textil wastewater	140 W 20 kHz 1 h 0 °C	85 % 120 min	[96]
TiO_2	CO_2 adsortion	40 kHz 4 h 25 °C	100 % 100 s	[97]
CeO_2	Methylene blue	100 W 60 min 40 °C	90 % 90 min	[98]
$Ho_2Sn_2O_7$	Eriochrome black T	60 W 15 min	95 % 120 min	[90]
$Ho_2Cu_2O_5/Ho_2O_3$	Eriochrome black T	45 W 30 min	93 % 120 min	[89]
Ce-TiO_2	Victoria blue	140 W 60 min	60.53 % 150 min	[86]
$TmVO_4/Fe_2O_3$	Eriochrome black T	60 W 30 min	68 % 120 min	[99]
$TmVO_4$	Methyl Violet	60 W 30 min	46.60 % 90 min	[100]
SnS_2/g-C_3N_4	Rhodamine B	200 W 50 min	98 % 120 min	[101]
Ag_2CrO_4/g-C_3N_4	Rhodamine B	200 W 40 min	96 % 120 min	[102]

6. Doping

Photocatalysis is a promising technology for degrading pollutants and generating clean energy, but it faces critical challenges that limit its practical efficiency. Conventional semiconductor materials, such as TiO_2, exhibit low absorption in the visible region of the solar spectrum, being restricted

predominantly to the ultraviolet (UV) range, which corresponds to only ~5% of solar irradiation [32,103]. This limitation drastically reduces their performance in real environmental conditions, where visible light is predominant [104]. Additionally, the rapid recombination of the electron-hole pairs generated compromises the efficiency of the process. After excitation by light, the charge carriers must remain separated long enough to take part in surface reactions, but they often recombine prematurely, dissipating energy as heat and reducing the production of reactive species [105].

Doping strategies have emerged as key approaches to overcoming these limitations. The controlled introduction of metallic (e.g., Ag, Fe^{3+}) or non-metallic elements (e.g., C, N, S) into TiO_2 modifies its electronic and structural properties, reducing the bandgap energy and extending photoactive absorption into the visible range. For instance, carbon doping decreases the bandgap from 2.13 eV to 0.54 eV, while nitrogen incorporation enhances photocatalytic efficiency under LED light by 4.3 times due to increased surface area and porosity [106,107]. Meanwhile, metallic dopants such as silver confer antimicrobial functionalities, and Fe^{3+} ions stabilize superhydrophilic properties, expanding applications in catalysis and smart materials [108,109]. These modifications also inhibit charge carrier recombination by creating trapping sites, extending the lifetime of electrons and holes and promoting the generation of oxidative radicals ($•O_2^-$, h^+), which are essential for contaminant degradation.

The analysis of the data presented in Table 4 reveals a significant variation in E_{gap} and doping load for different types of doped TiO_2. Egap values range from 1.93 eV for Co-S-TiO_2 to 3.22 eV for Ce-Sm-TiO_2 demonstrating how co-doping with different elements as a doping alternative can substantially change the electronic properties of the material [70,110].

Table 4. Metal/non-metal doping of TiO_2.

Photocatalyst	Precursor doppant	E_{gap} (eV)	Dopping load (%)	Reference
N-TiO_2	Triethylamine Natural extract	3.20	3 - 12	[111]
Fe-TiO_2	$Fe(NO_3)_3$ lawsonia inermis leaf extracts	2.70	7.0	[55]
Ag-TiO_2	$AgNO_3$ Mango leaf extract	2.75	2.5 – 3	[112]
Cu-TiO_2	$CuSO_4.5H_2O$ Mango leaf extract	3.05	0.5 – 2	[113]
Sr-TiO_2	Strontium acetate	3.16	1.0 – 5.0	[114]
Co-S-TiO_2	$CoCl_2$ Thiourea	1.93	0.2 for Co 0.69 – 2.06 for S	[70]
Ce-Sm-TiO_2	$Ce(NO_3)_3·6H_2O$ $Sm(NO_3)_3·6H_2O$	3.22	0.25 – 2.0	[110]
C-TiO_2	Glucose	2.82	0.5 – 4	[115]
S-TiO_2	Sulphuric acid		0.16 – 0.46	[116]
La-S-N-TiO_2	$La(NO_3)_3$ Thiourea	2.87	2.0 – 4.0	[117]
B-TiO_2	Boric acid	2.70	1.0 – 5.0	[118]

The doping load exhibits an extensive range of variation, oscillating between 0.1% and 7.0% in relation to the mass of iron and TiO_2 [55,119], demonstrating meticulous control in the incorporation of dopants during synthesis. This precision is fundamental, as excessive concentrations of dopants can induce metallization of the material and form a heterogeneous layer on the surface of the catalyst, uncharacterizing the doping process [120].

It is noteworthy that various natural precursors, such as extracts of mango leaves and henna, as well as the use of glucose, have been successfully used to improve the morphological characteristics of TiO_2 and to dope it with carbon [55,112,115], highlighting a growing trend towards more sustainable synthesis methods. The diversity of precursors and doping loads presented in the table reflects the ongoing effort of the scientific community to optimize the photocatalytic properties of TiO_2 through the manipulation of its electronic structure provided by the doping technique, with a view to applications in pollutant degradation and clean energy generation.

7. Strategies for characterizing photocatalytic materials

The comprehensive characterization of photocatalytic nanomaterials is a crucial step in understanding and optimizing their performance in environmental applications. Complementary analytical techniques, such as X-ray diffraction (XRD), scanning electron microscopy (SEM), UV-Vis diffuse reflectance spectroscopy, and B.E.T. surface area analysis, enable the synergistic investigation of essential physicochemical properties. While XRD identifies the crystalline structure and crystallite size, SEM reveals nanometric-scale morphology. Meanwhile, UV-Vis spectroscopy assesses optical properties, including bandgap energy, and B.E.T. analysis quantifies textural parameters such as surface area and porosity [121]. This integrated approach establishes correlations between synthesis methods and photocatalyst characteristics, such as particle distribution and electronic properties [122]. Such insights are fundamental for designing more efficient materials, with a direct impact on practical applications such as the degradation of emerging pollutants, water and air treatment, and sustainable energy generation ([123].

7.1 X-ray diffraction

The X-ray diffraction (XRD) technique is a fundamental tool for analyzing the crystal structure of materials. It explores the phenomenon of X-ray scattering, which occurs when a beam of X-rays interacts with the electrons of atoms in a crystal lattice, creating patterns of constructive and destructive interference. These diffraction patterns result in

characteristic peaks that can be analyzed to obtain essential information, such as the spacing between atomic planes, the composition of the phases present, the crystallographic orientation and the average size of the crystallites. XRD is a non-destructive technique applicable to a diverse range of materials, from solids to powders, thin films and nanomaterials, and is crucial in fields such as materials science, chemistry and physics [124].

To interpret diffraction patterns, Bragg's Law is used, which describes the condition necessary for constructive interference to occur (equation 1).

$$n\lambda = 2 * d * \text{sen}\theta \qquad \text{Eq. 1}$$

Where n is an integer (diffraction order), λ is the wavelength of the radiation, d is the spacing between the crystal planes and θ is the angle of incidence of the X-ray beam. By measuring the angles and intensities of the diffracted beams, it is possible to reconstruct the three-dimensional arrangement of the atoms in the material. To identify the phases present in the sample, the experimental data is compared with reference databases such as the ICDD (International Center for Diffraction Data). In addition, the technique can be adapted for studies under special conditions, such as variations in temperature or pressure, broadening its field of application [125].

The average crystallite size, a fundamental parameter in the characterization of polycrystalline and semi-crystalline materials, defines the dimensions of regions with periodic atomic ordering delimited by grain boundaries, constituting a critical factor for controlling macroscopic properties such as hardness, electrical conductivity and chemical reactivity [126]. The systematic reduction of this parameter enhances mechanical properties via the Hall-Petch mechanism, where grain contours act as barriers to the displacement of disagreements, while electrical properties induce a decrease in conductivity due to electronic scattering at the interfaces [127]. Parallel to this, materials with smaller crystallites exhibit greater specific surface area, enhancing adsorption phenomena and catalytic activity, particularly in nanostructured systems [128].

The conceptual distinction between crystallite (basic crystalline unit), grain (polycrystalline domain delimited by contours) and particle (discrete physical entity) becomes essential, where on nanometric scales crystallites and grains can present structural equivalence, while particles can encompass multiple grains or configure isolated single crystals (Fig. 7) - determining relations for applications in heterogeneous catalysis and functional materials [126].

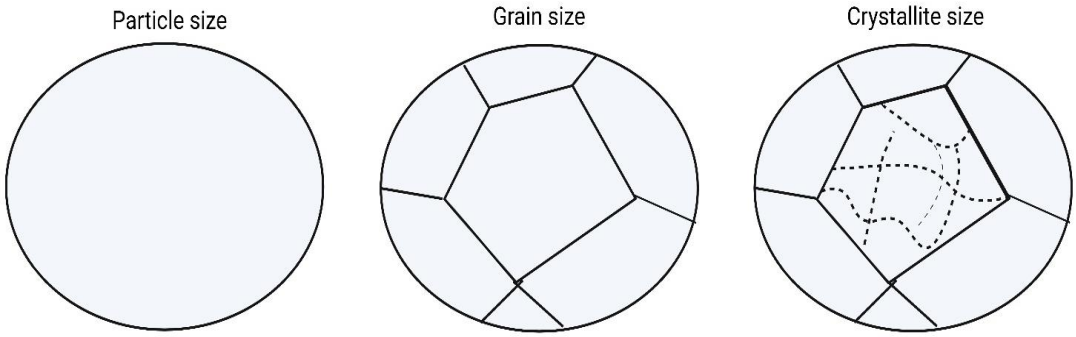

Fig. 7. Distinction between particle, grain and crystallite size (adapted by the author) [129].

The average crystallite size is commonly determined by XRD analysis using the Scherrer equation. This equation establishes a connection between the broadening of the diffraction peaks and the size of the crystallites, taking into account factors such as the wavelength of the X-ray radiation used, the width at half-height of the diffraction peak and the Bragg angle, as shown in equation 2.

$$D = \frac{K\lambda}{\beta cos\theta} \qquad \text{Eq. 2}$$

In this formula, D represents the average crystallite size, K is a constant that depends on the shape of the crystallite (usually 0.9), λ is the wavelength of the radiation used, β is the width at half-height (FWHM) of the peak corrected for instrumental broadening and θ is the Bragg angle.

The determination of lattice distortion in crystalline materials involves analyzing structural variations relative to the standard configuration of the pure crystalline material. This calculation is often performed using X-ray diffraction (XRD) techniques, which can identify and quantify imperfections in the crystal lattice. Lattice distortion can arise from various factors, such as internal stresses, point defects, or plastic deformations, and is expressed in terms of changes in the lattice parameters [130,131]. XRD data analysis provides insights into the broadening of diffraction peaks, which can be used to estimate distortion through methods such as the Scherrer equation for distortions (Equation 3).

$$\varepsilon = \frac{\beta}{4tan\theta} \qquad \text{Eq. 3}$$

Where ε is the lattice distortion (average strain), β is the half-height width of the corresponding peak and θ is the Bragg angle corresponding to the peak.

X-ray diffraction (XRD) stands out as an essential analytical method for investigating lattice distortions in crystalline materials, allowing precise quantification of

variations in lattice parameters caused by internal stresses, point defects or structural deformations [132]. In the case of TiO_2, the technique reveals critical nuances between its polymorphic phases (rutile and anatase), both tetragonal, but with different unit cell parameters: the rutile phase has a = b = 4.593 Å and c = 2.963 Å, while anatase has a = b = 3.79 Å and c = 9.51 Å [133,134]. These dimensional differences directly influence properties such as surface energy, band structure and density of electronic states, which are determining factors for photocatalytic applications [135]. Analysis of the broadening of diffraction peaks complements this study, providing quantitative data on microdeformations and crystallite size.

The assessment of crystallinity by XRD employs methods such as peak integration, which uses algorithms to decompose diffractograms into crystalline and amorphous components, calculating the proportion of each phase based on the area under the peaks [136]. This approach overcomes the limitations of qualitative analyses based solely on peak intensity, offering greater robustness for multiphase samples or those with overlapping signals, although it requires rigorous baseline correction and appropriate selection of fitting functions [137]. Studies of TiO_2 often reveal single- to three-phase materials, with anatase and rutile predominating due to their thermodynamic stability, while brookite occurs in smaller proportions [25,138]. Phase composition, which determines photocatalytic efficiency, correlates with specific structural characteristics of each polymorph, such as charge distribution and surface reactivity [139]. Thus, XRD is an indispensable tool for the rational design of materials with optimized properties for environmental and energy applications.

Table 5. Structural and crystalline properties of TiO_2-based photocatalysts.

Photocatalytic	Crystallite size (nm)	Phase composition (%)	Lattice deformation (%)	Crystallinity (%)	Reference
TiO_2	Anatase: 19.1 Rutile: 13.5	Anatase: 93.71 Rutile: 6.29	Anatase: 0.15 Rutile: 0.12	85	[140]
TiO_2	Anatase: 17.01 Brookite: 13.45 Rutile: 18.17	Anatase: 39 Brookite: 41 Rutile: 20	Anatase: 0.18 Brookite: 0.20 Rutile: 0.10	75	[25]
TiO_2	Anatase: 35 Rutile: 45	Anatase: 20.6 Rutile: 67.4	Anatase: 0.25 Rutile: 0.15	70	[141]
WO_3-TiO_2	Anatase: 51.5	Anatase: 100	Anatase: 0.10	90	[142]
Fe_3O_4/C/TiO_2	Anatase: 15.2 Magnetite: 9.2	Anatase: 77 Magnetite: 23	Anatase: 0.22 Magnetite: 0.30	80	[143]
SiO_2/TiO_2	Anatase: 5.0 Brookite: 5.0	Anatase: 81 Brookite: 19	Anatase: 0.35 Brookite: 0.40	65	[144]
TiO_2	Anatase: 5.1 Brookite: 9.3 Rutile: 18.2	Anatase: 13 Brookite: 24 Rutile: 63	Anatase: 0.40 Brookite: 0.30 Rutile: 0.18	60	[145]
TiO_2	Anatase: 26.9	Anatase: 100	Anatase: 0.12	95	[146]
TiO_2	Anatase: 4.5 Rutile: 17.0	Anatase: 16 Rutile: 84	Anatase: 0.45 Rutile: 0.20	55	[147]
TiO_2	Anatase: 17 Rutile: 15	Anatase: 77.2 Rutile: 32.8	Anatase: 0.20 Rutile: 0.25	75	[148]

7.2 B.E.T. surface area analysis

The B.E.T. technique, developed by Brunauer, Emmett and Teller in 1938, is an essential analytical method for determining the specific surface area of materials by physical adsorption of gases, based on three premises: adsorption in non-interactive multilayers, thermodynamic uniformity between layers, and applicability of the Langmuir isotherm for all layers [149]. The experimental protocol employs nitrogen as the adsorbed gas due to its chemical inertness and high purity, with measurements carried out at the gas condensation temperature (77 K) to ensure measurable adsorption, allowing the construction of isotherms that relate relative pressure (P/P_0) and adsorbed volume for precise calculation of the surface area [150]. This approach enables the characterization of critical parameters such as porosity, pore diameter and particle size distribution, and is widely applied in the quality control of nanostructured materials, catalysts and porous solids, where such properties determine functional performance in separation, catalysis and storage processes [151].

The BET technique has an important role to perform in the characterization of semiconductor oxides, offering a comprehensive view of their surface properties and consequently their photocatalytic potential. Table 6 shows a variety of surface area results for titanium dioxide, with values ranging from 124.5 to 934 m^2g^{-1}[152,153]. These results have a direct influence on photocatalytic efficacy, since larger surfaces facilitate more efficient reactions.

In the context of mitigating emerging contaminants, BET becomes a crucial tool for assessing the ability of materials to degrade organic pollutants under the action of sunlight. Larger surfaces are associated with better performance in air

and water purification. Thus, the BET technique is essential for the development of innovative solutions in the field of photocatalysis, optimizing the efficiency and applicability of semiconductor materials [123].

Table 6. Textural characterization of TiO_2-based photocatalysts.

Photocatalytic	Surface area (m^2g^{-1})	Pore diameter (nm)	Pore volume ($cm^3\ g^{-1}$)	Pore type	Key characteristics	Reference
TiO_2 pure	103.37	4.81	0.13	Mesoporous	Moderate porosity, good for small molecules	[154]
TiO_2 Anatase	245.51	4.36	0.30	Mesoporous	High surface area, excellent adsorption	[155]
TiO_2–ZnO/CS–Gr	37.97	37.97	0.23	Macroporous	Large pores for bulky compounds	[156]
Ce-TiO_2	135.23	28.75	0.35	Meso/Macro	Balanced structure, enhanced active sites	[153]
Ni-TiO_2	90.48	90.48	0.06	Macroporous	Very large pores, low efficiency	[157]
Ag-TiO_2	166.10	5.90	0.25	Mesoporous	Optimal for visible-light catalysis	[158]
TiO_2/CuO	87.50	9.70	0.08	Mesoporous	Moderate performance	[159]
TiO_2	10.80	28.48	0.99	Macroporous	Low area but high volume	[58]
TiO_2-Chitosan	71.92	125.09	0.23	Macroporous	Ultra-large pore structure	[160]
SC-TiO_2	217.00	6.65	0.37	Mesoporous	Best overall performance	[161]

7.3 UV-Vis spectroscopy with diffuse reflectance

Diffuse reflectance spectroscopy (DRS), a widely recognized instrumental technique in material studies, plays a crucial role in analyzing the optical properties of solid materials. Commonly used to investigate the bandgap energy (Egap) of semiconductors, such as metal-doped TiO_2 [162], DRS offers a non-destructive approach that does not require complex sample preparation or alter intrinsic material structures [163]. Based on the phenomenon of light scattering in multiple directions—predominant in rough surfaces or powdered materials where specular reflectance is minimal—DRS quantifies total reflectance by integrating both diffuse and specular components. This approach overcomes the limitations of Snell's Law, enabling accurate analysis of opaque or weakly absorbing materials [164,165]. It is particularly valuable for correlating microstructural characteristics (e.g., porosity, particle size) with optical properties, facilitating the study of light absorption mechanisms and charge transfer in systems such as heterostructures and hybrid catalysts [166,167]. The versatility of this technique, combined with its non-contact nature, establishes it as a key methodology for the rational optimization of materials used in heterogeneous photocatalysis, where understanding light-matter interactions is critical to catalytic performance.

The Kubelka-Munk model is a widely applied approach in DRS data analysis, enabling the transformation of reflectance data into a function that reflects the material's absorption properties [168]. The Kubelka-Munk equation, central to this transformation, is expressed in Equation 4:

$$F(R) = \frac{(1-R)^2}{2R} = \frac{K}{S} \qquad \text{Eq. 4}$$

Here, F(R) represents the Kubelka-Munk function, R is the diffuse reflectance, K denotes the absorption coefficient, and S symbolizes the scattering coefficient. These variables are employed to quantify the optical properties of the material. The significance of this equation lies in its ability to estimate the bandgap energy (E_{gap}) by plotting $[F(R)\cdot hv]^n$ against hv, where hv is the energy of the incident photon. The value of nnn varies according to the nature of the electronic transition, which can be direct or indirect, allowing for a deeper understanding of the electronic characteristics of semiconductors [169].

Conversely, the Tauc method provides an equally relevant alternative for the precise determination of Egap in semiconductor materials [170]. This method, primarily applied to materials with direct transitions, is expressed in Equation 5:

$$\alpha \cdot hv = A\left(hv - E_{gap}\right)^{n/2} \qquad \text{Eq. 5}$$

Here, α represents the absorption coefficient, hv is the incident photon energy, A is a constant dependent on the material's nature, E_{gap} is the desired bandgap energy, and n is a value that varies according to the type of electronic transition - direct or indirect. The linearization of the relationship between $(\alpha\cdot hv)^{2/n}$ and hv results in a Tauc plot, where extrapolating to the ordinate value equal to zero reveals E_{gap}. This technique enables a detailed and adjustable analysis, providing an efficient means to calibrate and optimize the optical properties of materials for photocatalytic applications [171].

The bandgap energy E_{gap} is a critical parameter in the evaluation of semiconductor materials, particularly in the field of photocatalysis, as it directly influences the efficiency with which a material can respond to light and initiate photocatalytic processes. The application of the Kubelka-Munk model and the Tauc method transforms diffuse

reflectance data into a metric that, when graphically represented, reveals E_{gap} through a graphical interpretation [172].

Table 7 presents a comprehensive and detailed compilation of bandgap energy values associated with photocatalytic performance and the source of incident radiation. It is important to highlight that lower bandgap values are highly desirable, as they enhance material activation under solar light exposure—an energy source that is both environmentally sustainable and economically advantageous [162,173].

Table 7. Optical properties and photocatalytic performance of TiO_2-based materials.

Photocatalyst	Visible light absorption (%)	Band gap (eV)	Photocatalytic conditions	Performance (%)	Reference
N-TiO_2/rGO	78-85	2.86	Visible light (LED) 120 min 25°C	78.29 Methylene blue	[174]
Bi_2O_3/TiO_2	75-82	2.80	Visible light 300 min pH 7	77.74 Methyl orange	[175]
Bi_2O_3/TiO_2	>90	2.70	Sunlight 100 min 30°C	99.0 Ciprofloxacin	[176]
Bi-TiO_2/ montmorillonite	85-88	2.80	UV-A (365 nm) 150 min	88.16 Rhodamine B	[177]
Ag-TiO_2	90-93	2.74	Solar simulator 180 min 1.5 AM	91.0 Phenol	[178]
Ce-TiO_2	80-85	2.40	Sunlight 360 min variable intensity	83.0 Diclofenac	[179]
ZnO–TiO_2/rGO	92-95	3.08	Sunlight 150 min [Catalyst] = 1 gL^{-1}	93.0 Malachite green	[180]
B–Sn/TiO_2	93-96	2.81	Sunlight 60 min [Dye] = 10 ppm	94.0 Congo red	[181]
Ce–B–TiO_2	97-99	2.24	UV-Vis 180 min 250W lamp	99.0 Tetracycline	[182]
Ag-TiO_2	90-95	2.32	Visible LED 120 min 50 $mWcm^{-2}$	92.98 Victoria blue	[183]

This preference for reduced bandgap energies is based on the material's ability to effectively utilize the abundant and constant natural light available, which not only reduces the total cost of the photocatalytic process, but also aligns the development of materials with a more sustainable paradigm for the degradation of organic pollutants and the improvement of water purification technologies, ensuring photocatalytic efficiency that harmonizes with current environmental and economic needs [28,162].

7.4 Scanning electron microscopy (SEM) and energy dispersive X-ray spectroscopy (EDS)

Scanning Electron Microscopy (SEM) has established itself as a high-precision analytical technique for characterizing materials on a nanometric scale, overcoming the limitations of conventional optical microscopy by employing a high-energy electron beam that interacts with the surface of the sample, generating signals such as secondary and backscattered electrons, which allow images to be obtained with magnifications of up to 300,000× and spatial resolution below 1 nm [184]. This capability enables the detailed investigation of critical parameters such as surface morphology, particle distribution, compositional heterogeneities and topographical features, particularly in semiconductor materials with photocatalytic properties [185].

The synergistic integration of SEM with Energy Dispersive Spectroscopy (EDS) constitutes a multimodal analytical platform, combining morphostructural evaluation with quantitative chemical mapping, essential for optimizing materials such as TiO_2 and ZnO - pure or combined in heterostructures - by monitoring post-synthesis microstructural modifications, identifying doping elements and analyzing interfaces in photocatalytic systems [186,187]. This multifunctional instrumental approach has proven indispensable in the rational development of high-efficiency photocatalysts, providing structural and chemical insights to enhance optical properties and surface reactivity.

Table 8 presents information on the particle size distribution and morphology of TiO_2 and TiO_2-based materials, highlighting the results obtained through SEM. Morphological characterization by SEM reveals a significant diversity of structures, from spherical nanoparticles to more complex structures such as nanocinths and nanoflowers [188–190] and particle sizes ranging from 5 nm to 300 nm. Particle size distribution is a crucial parameter that directly influences the

photocatalytic properties of the material. Smaller particles generally result in a larger specific surface area, providing more active sites for photocatalytic reactions [191].

Table 8. Particle size distribution and morphology of photocatalysts.

Photocatalyst	Average particle size (nm)	Morphology	Atomic composition (%)	Reference
TiO_2	45	Agglomerated cubic shapes	O (65.69) Ti (34.31)	[192]
Al-N-TiO_2/C	25	Meteorite shape	C (70.29) N (8.78) O (15.27) Al (3.47) Ti (2.19)	[193]
Co-WO_3	70 - 120	Agglomerated structure	Co (0.5)	[194]
Bi/BiOBr/TiO_2	5 - 300	Cubic	Bi (7.8) O (51.1) Br (6.9) Ti (34.2)	[195]
$BiFeO_3$/Bi_2O_3	100 - 400	Spherical	Bi (36.6) Fe (16.6) O (49.8) Ti (17.16)	[196]
ZnCdS	100 - 300	Conected nanoparticles	Zn (27.5) Cd (29.5) S (43.0)	[197]
$SrTiO_3$/TiO_2	150 - 300	Nanotubes	Ti (81.10) Sr (18.90)	[198]
Co-Sr-TiO_2	8	Nanoparticle	Co (9.82) Sr (1.82) Ti (13.23) O (75.13)	[199]
Mo-ZnO	13	Nanoparticle	Zn (61.37) O (34.42) Mo (4.21)	[200]
TiO_2	11.03	Spherical	Ti (60) O (40)	[201]

8. Photocatalytic applications

Photocatalytic materials are highlighted as a strategic technology for dealing with environmental and health challenges, with multifaceted applications ranging from decontamination of surfaces in critical environments (such as health units and industries) to advanced effluent treatment, where they have demonstrated efficacy in degrading recalcitrant contaminants such as drugs and endocrine disruptors, overcoming the limitations of conventional biological and physicochemical methods [202,203]. Its integration into existing systems increases the efficiency of treatment processes, reducing the use of chemical reagents and aligning with sustainability paradigms [204].

The ability to use solar irradiation as an energy source confers economic and environmental advantages, with recent research focused on the development of visible light-sensitive photocatalysts, whose optimization of quantum efficiency and operational stability has been achieved via strategies such as metal doping and the formation of heterojunctions, which modulate electronic properties and increase spectral absorption [205,206]. This convergence between the synthesis of functionalized materials and innovations in process engineering opens up prospects for scalable industrial applications, particularly in water management and sanitation, reinforcing the central role of these systems in the transition to environmentally responsible technologies [207].

8.1 Photocatalysis under the influence of LED light

LED (light-emitting diode) assisted photocatalysis is emerging as a disruptive technology, surpassing conventional methods by integrating high energy efficiency, low heat generation and extended service life [208]. The ability to modulate specific wavelengths makes it possible to optimize the activation of photocatalysts, directing chemical reactions with precision and spectral flexibility, including in the visible region [209]. This approach not only reduces operating costs, but also enables processes aligned with green chemistry, such as the degradation of pollutants in wastewater and the production of clean hydrogen [210], consolidating LEDs as a sustainable alternative to mercury UV lamps, which present toxicological risks and lower photonic efficiency [211,212].

Despite significant advancements, challenges persist regarding the spectral limitation of traditional photocatalysts, such as TiO_2, which primarily respond to UV radiation (5% of the solar spectrum). To extend absorption into the visible range (39% of the spectrum), strategies such as doping, heterojunction formation, and the development of hybrid catalysts have been prioritized [213,214]. These innovations aim to maximize electron-hole pair generation and quantum efficiency, which are essential for applications in high-value-added synthesis and industrial effluent decontamination [215]. Simultaneously, advancements in visible and near-infrared emissive LEDs reinforce the synergy between materials engineering and lighting technology, paving the way for energy-efficient systems [216].

The integration of LEDs into innovative photocatalytic reactors — such as microfluidic or tubular systems with homogeneous illumination [217] - has significantly enhanced mass transfer and light exposure, enabling scalable applications. The miniaturization of these devices supports

the development of portable solutions for water purification in remote areas and surface decontamination [218]. Furthermore, the use of LEDs eliminates the need for toxic components, such as mercury found in conventional lamps, thereby contributing to reduced environmental impact [219]. The next technological frontier lies in coupling tunable-bandgap photocatalysts with custom-spectrum LEDs, expanding their potential for green synthesis, air purification, and clean energy generation, in alignment with global sustainability and circular economy goals [215,217,220]. Table 9 presents photodegradation procedures under different experimental conditions influenced by LED light.

Table 9. Photodegradation efficiency of contaminants under LED system.

Photocatalysts	Contaminants	Irradiation parameters	Performance (%)	References
$BiVO_4$/Eco-graphene	Sulfamethoxazole	465 nm 68 W 8 h	57	[221]
Au-TiO_2	Metronidazole	365 and 395 nm 5-40 mW cm^{-2} 75 min	99	[220]
Au-ZnO	Rhodamine-6G	455 nm 15 min	97.8	[222]
Ni-zeolitic imidazolate framework-8	Methylene blue	365 nm 12 W 150 min	93.22	[223]
Co–ZnO	Ciprofloxacin	405-800 nm 150 W 60 min	98	[224]
TiO_2/rGO	Metolachlor	365 nm 200 W m^{-2} 120 min	100	[225]
$NiCo_2S_4$/chitosan	Congo red	White LED 23 W 52.13 W m^{-2} 60 min	93.46	[226]
Mn-WO_3	Diclofenac	550 nm 45 W cm^{-2} 180 min	88	[227]
Pt-TiO_2	Naproxen	365-450 nm 20 mW cm^{-2} 180 min	80	[228]
TiO_2	Ibuprofen	365 nm 210 mW cm^{-2} 20 min	97	[229]

It is noteworthy that the photocatalytic performance under the evaluated experimental conditions proved to be satisfactory, demonstrating the feasibility of the applied radiation source while also representing an energy-efficient alternative.

8.2 Photocatalysis under the influence of sunlight

Heterogeneous photocatalysis driven by sunlight is positioned as a multifunctional technology with environmental and energy applications. It stands out for its ability to degrade organic contaminants in aqueous matrices and convert light energy into clean fuels such as hydrogen [230]. This process, based on the activation of catalysts by solar radiation, eliminates dependence on artificial light sources, reducing operating costs and making economically competitive solutions feasible, especially in regions with high irradiance, such as Brazil [231]. In addition to wastewater decontamination, its application extends to sustainable energy production, in line with global decarbonization targets [232].

However, photocatalytic efficiency depends critically on the absorption of the solar spectrum, which is mostly composed of infrared (56%) and visible (39%), with only 5% of UV [233]. Conventional materials, such as TiO_2 anatase, are limited to UV absorption [234], which has led to strategies for reducing E_{gap}, such as doping with metals/non-metals, dye sensitization and semiconductor heterojunctions [235,236]. These modifications aim to extend the optical response to the visible, increasing the generation of electron-hole pairs and, consequently, the efficiency of pollutant degradation and H_2 production under sunlight [237].

For industrial scaling, challenges remain in the design of reactors that optimize light exposure and catalyst-contaminant interaction. Configurations such as compound parabolic collectors (CPC), thin-film spinning discs and flat plate reactors [238] look to maximize photonic efficiency, while the immobilization of catalysts on porous supports or fibres facilitates recovery and reuse [239]. The synergy between advances in materials science and process engineering is essential to overcome technical bottlenecks, consolidating solar photocatalysis as a scalable technology integrated into water and wastewater treatment systems [240]. Table 10 presents examples of photodegradation tests under the influence of sunlight.

Table 10. Solar light performance evaluation of photocatalysts.

Photocatalyst	Contaminant	Solar Irradiation Conditions	Reactor Type	Performance (%)	Geographical Location (Latitude / Longitude)	Reference
TiO_2	Volatile Organic Compounds (VOCs)	UV light (365 nm) 20 Wm^{-2} 60 min	Batch	~80.0	55.9533° N / 3.1883° W	[241]
Fe-modified TiO_2	Ibuprophen	Simulated solar light, 100 $mWcm^{-2}$ 120 min	Fixed-bed	95.0	37.9922° N / 1.1307° W	[242]
ZnO	Textile dyes	UV light (365 nm) 20 Wm^{-2} 180 min	Batch	90.0	53.5461° N / 113.4938° W	[243]
N-doped TiO_2	Phenol	Natural sunlight ~1000 Wm^{-2} 240 min	Continuous flow	85.0	19.4326° N / 99.1332° W	[238]
TiO_2/SnO_2	Organic dyes	UV light (365 nm) 25 Wm^{-2} 90 min	Batch	88.0	48.7758° N / 9.1829° E	[244]
TiO_2	Aromatic compounds	UV light (365 nm) 20 Wm^{-2} 120 min	Annular	92.0	48.8566° N / 2.3522° E	[245]
TiO_2/Graphene	Textile dyes	Simulated solar light 100 $mWcm^{-2}$ 150 min	Batch	87.0	46.0569° N / 14.5058° E	[229]
TiO_2	Organic compounds	UV light (365 nm) 30 Wm^{-2} 100 min	Continuous flow	90.0	51.9244° N / 4.4777° E	[240]
TiO_2/CdS	Organic dyes	Simulated solar light 100 $mWcm^{-2}$ 180 min	CPC	93.0	30.5728° N / 104.0668° E	[246]
N-TiO_2	Rhodamine	Simulated solar light 750.46 Wcm^{-2} 660 min	CTC	95.0	53.5461º N / 113.4938º O	[247]

The optimization of solar irradiation in photocatalytic processes goes beyond the mere availability of light, being intrinsically dependent on the configuration of solar reactors. These devices play a crucial role in concentrating incident solar radiation, thereby maximizing process efficiency. Additionally, geolocation emerges as a determining factor for the precise adjustment of operational parameters, such as treatment time and the angle of solar beam capture, as evidenced in previous studies [243, 248, 249].

8.3 Technological adaptation for industrial scale applications: Implementation strategies for photocatalytic systems in processing plants

Photocatalysts have emerged as a disruptive technology in water and wastewater treatment, establishing an unprecedented benchmark in the evolution of advanced oxidative processes. Their ability to trigger highly efficient chemical reactions under light irradiation, combined with minimal generation of toxic byproducts, introduces a new paradigm for the removal of emerging contaminants. In various application scenarios—ranging from the degradation of recalcitrant organic compounds to the inactivation of pathogens in water treatment systems—photocatalysis has demonstrated remarkable versatility and robustness, highlighting its potential for implementation in both wastewater treatment plants and industrial complexes [250].

Photocatalytic processes represent a strategic innovation in environmental management, combining sustainability with superior economic efficiency compared to traditional wastewater treatment methods. Their ability to operate under mild environmental conditions and degrade persistent pollutants, such as pharmaceuticals and pesticides, positions them as a viable solution for contemporary challenges [251]. The adaptability of these systems to diverse aqueous matrices—from industrial effluents to domestic sewage—has catalyzed scientific and industrial interest, indicating strong potential for large-scale adoption as a component of advanced treatment technologies [252].

However, transitioning to industrial applications requires overcoming technical challenges, such as developing reactors that maximize light exposure, optimize mass transfer, and enable continuous effluent flow [253]. Immobilizing photocatalysts onto solid supports (e.g., glass, concrete) replaces batch systems, facilitating scalability, while solar irradiation—particularly in tropical regions such as Brazil—reduces energy costs [254]. In treatment plants, photocatalysts immobilized in fixed-bed systems simplify disinfection and organic matter reduction, with proven

efficacy in pathogen inactivation under solar radiation [255,256]. The optimization of operational parameters (e.g., pH, flow rate) and pilot-scale studies (CONSTANTINO et al., 2022; MOLES et al., 2024) are essential to validate kinetic models and adapt the technology to real-world scenarios, consolidating it as a technically robust and environmentally integrated solution.

Scaling up photocatalysis from laboratory to industrial levels requires harmonizing critical variables such as energy efficiency, reactor design for high flow rates, and compatibility with existing infrastructure. Parameters such as catalytic plate geometry, flow velocity, and effluent recirculation demand precise computational modeling, while intermediate-scale testing validates performance and mitigates operational risks [257]. The synergistic combination with conventional methods—such as pre-treatment to enhance the biodegradability of complex effluents [248] or post-treatment to degrade recalcitrant pollutants [258] maximizes treatment efficiency, adapting to dynamic matrices such as domestic sewage and industrial waste [259].

Industrial feasibility depends on interdisciplinary approaches integrating materials engineering, environmental chemistry, and process optimization [260]. The synthesis of highly stable and reusable nanostructured catalysts [261], combined with dynamic control of variables (e.g., pH, flow rate) via artificial intelligence algorithms, ensures efficiency in complex operational scenarios. These advancements go beyond complementary applications, positioning photocatalysis as the core of sustainable water management systems, where technical performance converges with circular economy principles and energy consumption reduction. Table 11 presents representative examples of technological applications of photocatalysts employed in integrated approaches for the treatment of effluents from diverse sources.

Table 11. Complementary techniques to photocatalysis in wastewater treatment.

Photocatalysts	Combined Treatment	Effluent	Removal efficiency (%)	References
ZnO/ZnO-GO	Coagulation-flocculation; sand-based filtration	Textile wastewater	COD: 70.24 BOD: 54.94	[262]
TiO_2	Coagulation-flocculation	Hospital wastewater	COD: 95.0 BOD: 90.0	[263]
TiO_2	Ozonation	Textile wastewater	COD: 91.5 BOD: 94.0	[264]
Black sand	Adsorptive filtration	Textile wastewater	COD: 50.40	[265]
TiO_2	phytoremediation	landfill leachate	COD: 68.48 BOD: 60.53	[266]
ZnO	Ultrasound process	Poultry slaughterhouse wastewater	NH_4^+: 35.15	[267]
SnO_2	Filtration and biological treatment	Petroleum refinery wastewater	COD: 73.16	[268]
Fe–TiO_2	Coagulation-flocculation	Municipal Wastewater	COD: 85.0	[269]
g-C_3N_4	Biological treatment and CPC reactor	Hospital wastewater	COD: 56.0 BOD: 29.0	[270]
TiO_2	Filtration and biological treatment	Textile wastewater	COD: 70.0	[271]

The integration of conventional and advanced treatment methods can enhance the mitigation of recalcitrant and toxic contaminants, whose effective removal is often not achieved through isolated or low-efficiency techniques [272–275].

8.4 Functionalized antimicrobial coatings

Photocatalysts have occupied a prominent position in nanotechnology applied to architecture and materials engineering, mainly due to their extraordinary photocatalytic properties. The incorporation of nanometer-scale photocatalysts into architectural surfaces, such as mortars, paints and coatings, gives them innovative self-cleaning characteristics and antimicrobial activity, transforming the way maintenance is carried out and sustainability is sought in buildings [276]. When exposed to UV radiation, the nanoparticles of these materials trigger photocatalytic reactions that generate superhydrophilic surfaces, capable of decomposing organic compounds and resisting the action of external agents [277]. This process not only protects the aesthetic and functional integrity of the materials, but also drastically reduces the need for manual cleaning interventions.

In the hospital sector, photocatalytic paints are a technological innovation of significant importance, especially due to their antimicrobial and self-cleaning properties. These characteristics are afforded by the incorporation of photocatalysts in their composition, which, under the action of light, induce chemical reactions capable of degrading atmospheric pollutants, eliminating stains and neutralizing pathogenic microorganisms present in the air [278]. These properties make these coatings particularly suitable for healthcare environments, where infection control is a priority, while contributing to the reduction of volatile organic compounds and the dissipation of odours, ensuring more hygienic and safer spaces. The application of these paints to hospital surfaces is a promising strategy not only for air purification, but also for the sterilization of surgical instruments, since their efficiency in degrading organic molecules and inactivating microorganisms meets the strict asepsis standards required in these environments [279]. Recent studies have shown, for example, that photocatalytic films applied to hospital surfaces favor self-cleaning and the inactivation of bacteria such as Escherichia coli when exposed to ultraviolet radiation [280].

In modern dentistry, photocatalysts are revolutionizing dental bleaching by degrading organic pigments under light exposure while preserving enamel integrity. Photocatalytic nanoparticles incorporated into dental materials confer stain resistance and self-cleaning properties, in addition to enhancing oxidation reactions under UV light [281], thereby

minimizing invasive procedures and ensuring superior aesthetic outcomes. Studies also associate these compounds with reduced bacterial biofilm formation, lowering the risk of cavities and periodontal diseases [282]. Recent advancements include bleaching gels with lower hydrogen peroxide concentrations—capable of generating free radicals under light without inducing sensitivity—while maintaining both efficacy and safety [283]. This technology is setting new standards in aesthetic dentistry by integrating whitening performance with tissue preservation [218], solidifying photocatalysis as both a clinical and preventive strategy. Table 12 presents examples of photocatalytic activity applications aimed at the inactivation and mitigation of pathogenic organisms, considering different configurations and application strategies.

The data highlight the high application potential of photocatalysts in the inactivation of various pathogenic microorganisms, enabling their use in critical environments such as hospital settings, areas with high toxic loads, and air purification and HVAC systems. Furthermore, the effectiveness of the process under low-power LED irradiation underscores its viability as an energy-efficient and sustainable alternative for large-scale decontamination processes [293–298].

Table 12. Antimicrobial and antifungal activity of selected photocatalysts.

Photocatalysts	Pathogen	Irradiation parameters	Inactivation (%)	References
TiO_2	Hyphae	LED visible light 120 min	45.0	[284]
Ag-ZnO	C. albicans	LED visible light 120 min	99.0	[285]
C-TiO_2	B. subtilis	Daylight LED bulb 120 min	100.0	[286]
Ag-TiO_2	E. Coli	Xenon lamp 50 $mWcm^{-2}$ 120 min	96.7	[287]
B-CarbonQD-C_3N_4	E. Coli	Sunlight 90 min	100.0	[288]
Cu-TiO_2	Streptococcus mutans	visible light source 120 min	99.89	[289]
N–Ag/TiO_2/ZnO	C. albicans	UV-A 15 min	99.0	[290]
N-TiO_2	Staphylococcus aureus	Fluorescent lamp 720 min	99.99	[291]
ZnO	E. Coli	LED visible light 1440 min	99.9	[292]

9. Conclusions

This review highlights the significant advancements in the field of semiconductor photocatalysis, particularly focusing on titanium dioxide (TiO_2) and its modified forms as multifunctional materials for environmental remediation and sustainable energy applications. Through a comprehensive analysis of synthesis routes, such as sol-gel, hydrothermal, and ultrasonic methods, it becomes evident that precise control over morphological and structural features is essential to enhancing photocatalytic performance. Doping strategies, heterojunction formation, and the integration of green synthesis approaches using agro-industrial residues have emerged as effective pathways to extend light absorption into the visible spectrum and improve charge carrier dynamics.

Advanced characterization techniques, including XRD, B.E.T., SEM/EDS, and UV-Vis spectroscopy, have provided deep insights into the correlation between crystallinity, surface area, optical properties, and photocatalytic efficiency. The materials discussed herein demonstrate promising potential in various applications, from the degradation of emerging pollutants and antimicrobial coatings to solar-driven hydrogen production and hybrid wastewater treatment systems. Notably, the use of LED irradiation and solar reactors reveals scalable solutions for integrating photocatalysis into real-world water and sanitation infrastructure.

Nonetheless, challenges such as low quantum efficiency under visible light, limited long-term catalyst stability, and scale-up constraints remain. Addressing these issues will require interdisciplinary approaches that combine material science innovation, reactor engineering, and smart process control—potentially guided by artificial intelligence. Looking forward, the development of adaptable, high-performance photocatalytic systems aligned with circular economy principles could play a pivotal role in advancing global environmental sustainability.

Acknowledgments

The authors gratefully acknowledge the financial support provided by the Coordination for the Improvement of Higher Education Personnel (CAPES) and the National Council for Scientific and Technological Development (CNPq). We also extend our sincere gratitude to the Federal University of Western Bahia (UFOB) and the Graduate Program in Pure and Applied Chemistry (POSQUIPA) for providing the essential infrastructure and academic environment required for this research. This work would not have been possible without the invaluable support of these institutions.

Author Contributions

Yago Kaic de Souza França – Literature review and manuscript drafting. Danilo Rodrigues de Souza – Critical analysis and theoretical contribution. Kauê Sodré Pereira – Text translation and language editing. Yasmin Hozana Carvalho Feitosa – Table Design and Formatting. Vitor

Barbosa Marques – Figures preparation and editing.

References and Notes

[1] Stoett, P.; Scrich, V. M.; Elliff, C. I.; Andrade, M. M.; de M. Grilli, N.; Turra, A. *World Dev.* **2024**, *184*, 106756. [Crossref]

[2] Das, S.; Parida, V. K.; Tiwary, C. S.; Gupta, A. K.; Chowdhury, S. In *Bioremediation of Emerging Contaminants in Water. Volume 1*; ACS Symposium Series; American Chemical Society, 2024; Vol. 1475, p 1. [Crossref]

[3] Shanmuganathan, R.; Sibtain Kadri, M.; Mathimani, T.; Hoang Le, Q.; Pugazhendhi, A. *Chemosphere* **2023**, *332*, 138812. [Crossref]

[4] Masinga, P.; Simbanegavi, T. T.; Makuvara, Z.; Marumure, J.; Chaukura, N.; Gwenzi, W. *Environ. Monit. Assess.* **2024**, *196*, 367. [Crossref]

[5] Xu, B. J.; Lu, Y.; Liu, N.; Chen, Y.; Liu, M.; Wu, Q. Y.; Du, Y. *Environ. Sci. Technol.* **2024**, *58*, 22064. [Crossref]

[6] Nehme, T. M.; Martins, G. E. C.; Calvelli, J. M. F. F. B.; Santos, L. V. de S. *Contam. emergentes uma visão ecotoxicológica sobre o impacto dos fármacos no meio Ambiente e na saúde pública*. Editora Atena, 2023, p. 11. [Crossref]

[7] Wang, F.; Xiang, L.; Sze-Yin Leung, K.; Elsner, M.; Zhang, Y.; Guo, Y.; Pan, B.; Sun, H.; An, T.; Ying, G.; Brooks, B. W.; Hou, D.; Helbling, D. E.; Sun, J.; Qiu, H.; Vogel, T. M.; Zhang, W.; Gao, Y.; Simpson, M. J.; Luo, Y.; Chang, S. X.; Su, G.; Wong, B. M.; Fu, T. M.; Zhu, D.; Jobst, K. J.; Ge, C.; Coulon, F.; Harindintwali, J. D.; Zeng, X.; Wang, H.; Fu, Y.; Wei, Z.; Lohmann, R.; Chen, C.; Song, Y.; Sanchez-Cid, C.; Wang, Y.; El-Naggar, A.; Yao, Y.; Huang, Y.; Cheuk-Fung Law, J.; Gu, C.; Shen, H.; Gao, Y.; Qin, C.; Li, H.; Zhang, T.; Corcoll, N.; Liu, M.; Alessi, D. S.; Li, H.; Brandt, K. K.; Pico, Y.; Gu, C.; Guo, J.; Su, J.; Corvini, P.; Ye, M.; Rocha-Santos, T.; He, H.; Yang, Y.; Tong, M.; Zhang, W.; Suanon, F.; Brahushi, F.; Wang, Z.; Hashsham, S. A.; Virta, M.; Yuan, Q.; Jiang, G.; Tremblay, L. A.; Bu, Q.; Wu, J.; Peijnenburg, W.; Topp, E.; Cao, X.; Jiang, X.; Zheng, M.; Zhang, T.; Luo, Y.; Zhu, L.; Li, X.; Barceló, D.; Chen, J.; Xing, B.; Amelung, W.; Cai, Z.; Naidu, R.; Shen, Q.; Pawliszyn, J.; Zhu, Y. guan; Schaeffer, A.; Rillig, M. C.; Wu, F.; Yu, G.; Tiedje, J. M. *Innovation* **2024**, *5*, 100612. [Crossref]

[8] Puri, M.; Gandhi, K.; Kumar, M. S. *J. Environ. Manage.* **2023**, *332*, 117344. [Crossref]

[9] PUBMED. *Emerging Contaminants (2019 - 2025)*. Avaliable from: https://pubmed.ncbi.nlm.nih.gov/?term=emerging+contaminants&filter=years.2010-2024&timeline=expanded. Access May 2025.

[10] Disner, G. R.; Tareq, S. M. *Front. Water* **2025**, *7*, 2023. [Crossref]

[11] Li, X.; Shen, X.; Jiang, W.; Xi, Y.; Li, S. *Ecotoxicol. Environ. Saf.* **2024**, *278*, 116420. [Crossref]

[12] Levin, R.; Villanueva, C. M.; Beene, D.; Cradock, A. L.; Donat-Vargas, C.; Lewis, J.; Martinez-Morata, I.; Minovi, D.; Nigra, A. E.; Olson, E. D.; Schaider, L. A.; Ward, M. H.; Deziel, N. C. *J. Expo. Sci. Environ. Epidemiol.* **2024**, *34*, 3. [Crossref]

[13] Senthil Rathi, B.; Senthil Kumar, P.; Parthasarathy, V.; Gokul, R.; Dharani, R.; Lavanya, R.; Rangasamy, G. *Water Pract. Technol.* **2024**, *19*, 3154. [Crossref]

[14] Zhou, Q.; Chen, H.; Liu, G.; Wang, X. *Front. Environ. Sci.* **2024**, *12*, 1. [Crossref]

[15] Zahmatkesh, S.; Bokhari, A.; Karimian, M.; Zahra, M. M. A.; Sillanpää, M.; Panchal, H.; Alrubaie, A. J.; Rezakhani, Y. *Environ. Monit. Assess.* **2022**, *194*, 884. [Crossref]

[16] Haider Jaffari, Z.; Jeong, H.; Shin, J.; Kwak, J.; Son, C.; Lee, Y.-G.; Kim, S.; Chon, K.; Hwa Cho, K. *Chem. Eng. J.* **2023**, *466*, 143073. [Crossref]

[17] Steephen, A.; V, P.; B, A.; R, P.; Reddy P, R.; M, S.; Kumar M, S. *Int. J. Hydrogen Energy* **2024**, *52*, 1393. [Crossref]

[18] Jasemizad, T.; Malmström, J.; Padhye, L. P. *Environ. Sci. Water Res. Technol.* **2024**, *10*, 1256. [Crossref]

[19] Hsu, C. Y.; Mahmoud, Z. H.; Abdullaev, S.; Ali, F. K.; Ali Naeem, Y.; Mzahim Mizher, R.; Morad Karim, M.; Abdulwahid, A. S.; Ahmadi, Z.; Habibzadeh, S.; kianfar, E. *Case Stud. Chem. Environ. Eng.* **2024**, *9*, 100626. [Crossref]

[20] Datta, P.; Roy, S. *Catal. Res.* **2023**, *03*, 20. [Crossref]

[21] Ren, G.; Han, H.; Wang, Y.; Liu, S.; Zhao, J.; Meng, X.; Li, Z. *Nanomater. (Basel, Switzerland)* **2021**, *11*, 1804. [Crossref]

[22] Munawar, T.; Sardar, S.; Mukhtar, F.; Nadeem, M. S.; Manzoor, S.; Ashiq, M. N.; Khan, S. A.; Kocc, M. *Phisical Chem. Chem. Phisics* **2023**, *25*, 17. [Crossref]

[23] Zhang, J.; Wu, H.; Shi, L.; Wu, Z.; Zhang, S.; Wang, S.; Sun, H. *Sep. Purif. Technol.* **2024**, *329*, 125225. [Crossref]

[24] Saleh, M. R.; El-Bery, H. M.; Abdelhamid, H. N. *Appl. Organomet. Chem.* **2023**, *37*, 1. [Crossref]

[25] Kim, M. G.; Kang, J. M.; Lee, J. E.; Kim, K. S.; Kim, K. H.; Cho, M.; Lee, S. G. *ACS Omega* **2021**, *6*, 10668. [Crossref]

[26] Valencia, S.; Marín, J. M.; Restrepo, G. *Open Mater. Sci. J.* **2010**, *4*, 9. [Crossref]

[27] Sadia, S. I.; Shishir, M. K. H.; Ahmed, S.; Aidid, A. R.; Islam, M. M.; Rana, M. M.; Al-Reza, S. M.; Alam, M. A. *South African J. Chem. Eng.* **2024**, *50*, 51. [Crossref]

[28] Thakur, S.; Ojha, A.; Kansal, S. K.; Gupta, N. K.; Swart, H. C.; Cho, J.; Kuznetsov, A.; Sun, S.; Prakash, J. *Adv. Powder Mater.* **2024**, *3*, 100233. [Crossref]

[29] Kistan, A.; Mohan, S.; Mahalakshmi, S.; Jayanthi, A.; Ramya, A. J.; Karthik, P. S. *Main Gr. Chem.* **2024**, *23*, 17. [Crossref]

[30] Emrie, D. B. *J. Nanomater.* **2024**, *2024*, 6109770. [Crossref]

[31] Albaidani, K.; Timoumi, A.; Belhadj, W.; Alamri, S. N.; Ahmed, S. A. *Ceram. Int.* **2023**, *49*, 36265. [Crossref]

[32] Singh, S.; Rai, N.; Tiwari, H.; Gupta, P.; Verma, A.; Kumar, R.; Kailashiya, V.; Salvi, P.; Gautam, V. *ACS Appl. Bio Mater.* **2023**, *6*, 3577. [Crossref]

[33] Srujana, T. L.; Rao, K. J.; Korumilli, T. *ACS Biomater. Sci. Eng.* **2025**, *11*, 1291. [Crossref]

[34] Gavrilescu, M.; Demnerová, K.; Aamand, J.; Agathos, S.; Fava, F. *N. Biotechnol.* **2015**, *32*, 147. [Crossref]

[35] Danks, A. E.; Hall, S. R.; Schnepp, Z. *Mater. Horizons* **2016**, *3*, 91. [Crossref]

[36] Thanh, N. T. K.; Maclean, N.; Mahiddine, S. *Chem. Rev.* **2014**, *114*, 7610. [Crossref]

[37] Şahin, İ.; Özbakır, Y.; İnönü, Z.; Ulker, Z.; Erkey, C. *Gels*. **2018**, *4*, 3. [Crossref]

[38] Phromma, S.; Wutikhun, T.; Kasamechonchung, P.; Eksangsri, T.; Sapcharoenkun, C. *Applied Sciences* **2020**, *10*, 993. [Crossref]

[39] Hosseinzadeh Kouhi, P.; Darab, M.; Ashiri, R. *Ceram. Int.* **2024**, *50*, 26938. [Crossref]

[40] Esposito, S. *Mater. (Basel, Switzerland)* **2019**, *12*, 668. [Crossref]

[41] Bokov, D.; Turki Jalil, A.; Chupradit, S.; Suksatan, W.; Javed Ansari, M.; Shewael, I. H.; Valiev, G. H.; Kianfar, E. *Adv. Mater. Sci. Eng.* **2021**, *2021*, ID 5102014. [Crossref]

[42] de Lima, O. J.; de Araújo, D. T.; Marçal, L.; Crotti, A. E. M.; Machado, G. S.; Nakagaki, S.; de Faria, E. H.; Ciuffi, K. J. *ChemEngineering* **2022**, *6*, 55. [Crossref]

[43] Styskalik, A.; Skoda, D.; Barnes, C. E.; Pinkas, J. *Catalysts* **2017**, *7*, 168. [Crossref]

[44] Parashar, D.; Achari, G.; Kumar, M. *Chemosphere* **2023**, *341*, 140025. [Crossref]

[45] Stoyanova, A.; Hitkova, H.; Kaneva, N.; Bachvarova-Nedelcheva, A.; Iordanova, R.; Marinovska, P. *Catalysts* **2024**, *14*, 469. [Crossref]

[46] Abodlal, R. *Res. Sq.* **2024**, 1

[47] Mantilla, A.; Samaniego Benitez, E.; Montes Valenzuela, I.; Romero Ortiz, G.; Cipagauta Díaz, S.; Lartundo Rojas, L.; Javier Tzompantzi Morales, F.; Navarrete Magaña, M. *J. Photochem. Photobiol. A Chem.* **2025**, *459*, 116079. [Crossref].

[48] El Mouchtari, E. M.; El Mersly, L.; Belkodia, K.; Piram, A.; Lebarillier, S.; Briche, S.; Rafqah, S.; Wong-Wah-Chung, P. *Toxics*. **2023**, *11*, 299. [Crossref]

[49] Yasmeen, S.; Burratti, L.; Duranti, L.; Sgreccia, E.; Agresti, A.; Prosposito, P. *Applied Sciences* **2025**, *15*, 1899. [Crossref]

[50] Saridewi, N.; Rustanti, S.; Zulys, A.; Nurbayti, S.; Aziz, I.; Adawiah, A. *Bull. Chem. React. Eng. Catal.* **2023**, *18*, 375. [Crossref]

[51] Ben Amor, I.; Hemmami, H.; Laouini, S. E.; Mahboub, M. S.; Barhoum, A. *Catalysts* **2022**, *12*, 1611. [Crossref]

[52] Alhadhrami, A.; Mohamed, G. G.; Sadek, A. H.; Ismail, S. H.; Ebnalwaled, A. A.; Almalki, A. S. A. *Materials (Basel)* **2022**, *15*, 8211.[Crossref]

[53] Leroy, S.; Blach, J.-F.; Kopia, A.; Lech, S.; Cieniek, Ł.; Kania, N.; Saitzek, S. *J. Photochem. Photobiol. A Chem.* **2022**, *426*, 113739. [Crossref]

[54] Haruna, S. S. B. Z.; Hussina, W. N. W. S. R.; Hairomd, N. H. H.; Basrie, N. H. K. H.; Raslie, N. I.; Rosmanc, A.; Ainuddinb, M. R. J. A. R. *ASEAN Eng. J.* **2023**, *13*, 141. [Crossref]

[55] Singh, S. K.; Avasarala, S.; S, M.; Bose, S. *ACS Sustain. Resour. Manag.* **2024**, *1*, 1501. [Crossref]

[56] Faisal, S.; Jan, H.; Shah, S. A.; Shah, S.; Khan, A.; Akbar, M. T.; Rizwan, M.; Jan, F.; Wajidullah; Akhtar, N.; Khattak, A.; Syed, S. *ACS Omega* **2021**, *6*, 9709. [Crossref]

[57] Singh, H.; Desimone, M. F.; Pandya, S.; Jasani, S.; George, N.; Adnan, M.; Aldarhami, A.; Bazaid, A. S.; Alderhami, S. A. *Int. J. Nanomedicine* **2023**, *18*, 4727. [Crossref]

[58] Lal, M.; Sharma, P.; Singh, L.; Ram, C. *Results Eng.* **2023**, *17*, 100890. [Crossref]

[59] Ejsmont, A.; Goscianska, J. *Mater. (Basel, Switzerland)* **2023**, *16*, 1641. [Crossref]

[60] de Luciano, G. B.; Soto-Cruz, B. S.; Romero-López, A.; Panecatl-Bernal, Y.; Luna-López, J. A.; Domínguez-Jiménez, M. Á. *Appl. Nano* **2024**, *5*, 58. [Crossref]

[61] Jayatissa, Y. X. G. A. H.; Yu, Z.; Chen, X.; Li, M. *J. Nanomater.* **2020**, *2019*, NA.

[62] Zhu, H.; He, X.; Xu, Z.; Dai, L. *Green Chem.* **2025**, *27*, 1278. [Crossref]

[63] Verki, M. T.; Halladj, R.; Habibzadeh, S.; Shalmani, F. M. *Sci. Rep.* **2025**, *15*, 6301. [Crossref]

[64] Kamata, K.; Aihara, T.; Wachi, K. *Chem. Commun.* **2024**, *60*, 11483. [Crossref]

[65] de Conti, M. C. M. D.; Dey, S.; Pottker, W. E.; La Porta, F. A. *Mater. Today Sustain.* **2023**, *23*. [Crossref]

[66] Yang, G.; Park, S.-J. *Materials*. **2019.** [Crossref]

[67] Nandihalli, N.; Gregory, D. H.; Mori, T. *Adv. Sci.* **2022**, *9*, 2106052. [Crossref]

[68] Ndlwana, L.; Raleie, N.; Dimpe, K. M.; Ogutu, H. F.; Oseghe, E. O.; Motsa, M. M.; Msagati, T. A. M.; Mamba, B. B. *Mater. (Basel, Switzerland)* **2021**, *14*, 5094. [Crossref]

[69] Saqib, M.; Rahman, N.; Safeen, K.; Mekkey, S. D.; Salem, M. A.; Safeen, A.; Husain, M.; Zaman, S. u; Abdullaev, S.; Kalsoom, A.; El-Bahy, Z. M.; Khan, R. *J. Mater. Res. Technol.* **2023**, *26*, 8048. [Crossref]

[70] Jiang, Z.; Yang, F.; Yang, G.; Kong, L.; Jones, M. O.; Xiao, T.; Edwards, P. P. *J. Photochem. Photobiol. A Chem.* **2010**, *212*, 8. [Crossref]

[71] Hameed, H. G.; Abdulrahman, N. A. *Phys. Chem. Res.* **2023**, *11*, 771. [Crossref]

[72] Alaizeri, Z. M.; Alhadlaq, H. A.; Aldawood, S.; Akhtar, M. J.; Aziz, A. A.; Ahamed, M. *Molecules* **2023**, *28*, 5153.

[73] Bazzanella, N.; Bajpai, O. P.; Fendrich, M.; Guella, G.; Miotello, A.; Orlandi, M. *MRS Commun.* **2023**, *13*, 1252. [Crossref]

[74] Kubiak, A.; Cegłowski, M. *Sci. Rep.* **2024**, *14*, 1. [Crossref]

[75] Nassar, M. Y.; NourEldien, M. S.; Ibrahim, I. M.; Aly, H. M. *Processes* **2023**, *11*, 1322. [Crossref]

[76] Nguyen, K. T.; Nguyen, C. T. H.; Pham, C. N.; Duong, L. T.; Nguyen, B. Q.; Le, H. B.; Nguyen, M. V. N.; Dao, N. N. *Res. Chem. Intermed.* **2023**, *49*, 57. [Crossref]

[77] Jabeen, S.; Ganie, A. S.; Bala, S.; Khan, T. *Mater. Poceedings* **2023**, *14*, 6. [Crossref]

[78] Kumar, A.; Kuang, Y.; Liang, Z.; Sun, X. *Mater. Today Nano* **2020**, *11*, 100076. [Crossref]

[79] Matussin, S. N.; Khan, F.; Harunsani, M. H.; Kim, Y. M.; Khan, M. M. *ACS Omega* **2024**, *9*, 16420. [Crossref]

[80] Menon, K.; Lopis, A. D.; Choudhari, K. S.; Kulkarni, B.; Maradur, S.; Kulkarni, S. D. *Mater. Res. Bull.* **2025**, *181*, 113074. [Crossref]

[81] Nawaz, R.; Ullah, H.; Ghanim, A. A. J.; Irfan, M.; Anjum, M.; Rahman, S.; Ullah, S.; Abdel Baki, Z.; Kumar Oad, V. *ACS Omega* **2023**, *8*, 36076. [Crossref]

[82] Oturan, M. A.; Aaron, J.-J. *Crit. Rev. Environ. Sci. Technol.* **2014**, *44*, 2577. [Crossref]

[83] Yusof, N. S. M.; Anandan, S.; Sivashanmugam, P.; Flores, E. M. M.; Ashokkumar, M. *Ultrason. Sonochem.* **2022**, *85*, 105988. [Crossref]

[84] Stopic, S.; Wenz, F.; Husovic, T.-V.; Friedrich, B. *Metals*. **2021**, *11*, 463. [Crossref]

[85] Dey, A.; Gogate, P. R. *Environ. Qual. Manag.* **2024**, *33*, 3. [Crossref]

[86] Yu, Y.; Mei, Y.; Wei-jie, Q.; Hai-hong, B.; Hong-zhuo, L.; and Che, J. *Int. J. Nanomedicine* **2023**, *18*, 1321. [Crossref]

[87] Sancheti, S. V; Gogate, P. R. *Ultrason. Sonochem.* **2017**, *36*, 527. [Crossref]

[88] Haghighi, A.; Rahemi, N.; Fatehifar, E.; Shabani, M. *J. Environ. Chem. Eng.* **2023**, *11*, 109601. [Crossref]

[89] Mahdi, M. A.; Talebzadeh, Z.; Ganduh, S. H.; Mohmmad Burhan, Z.; Jasim, L. S.; Salavati-Niasari, M. *Arab. J. Chem.* **2023**, *16*, 105282. [Crossref]

[90] Trinh, Q. T.; Golio, N.; Cheng, Y.; Cha, H.; Tai, K. U.; Ouyang, L.; Zhao, J.; Tran, T. S.; Nguyen, T.-K.; Zhang, J.; An, H.; Wei, Z.; Jerome, F.; Amaniampong, P. N.; Nguyen, N.-T. *Green Chem.* **2025**, *27*, 4926. [Crossref]

[91] Izadifar, Z.; Babyn, P.; Chapman, D. *J. Med. Biol. Eng.* **2019**, *39*, 259. [Crossref]

[92] Devos, C.; Bampouli, A.; Brozzi, E.; Stefanidis, G. D.; Dusselier, M.; Van Gerven, T.; Kuhn, S. *Chem. Soc. Rev.* **2025**, *54*, 85. [Crossref]

[93] Wong, C. C. Y.; Raymond, J. L.; Usadi, L. N.; Zong, Z.; Walton, S. C.; Sedgwick, A. C.; Kwan, J. *Ultrason. Sonochem.* **2023**, *99*, 106559. [Crossref]

[94] Anandan, S.; Sivasankar, T.; Lana-Villarreal, T. *Ultrason. Sonochem.* **2014**, *21*, 1964. [Crossref]

[95] Dey, A.; Korde, S.; Gogate, P. R.; Agarkoti, C. *Ultrason. Sonochem.* **2023**, *96*, 106426. [Crossref]

[96] Karapnar, M.; Gürkan, S.; Alper Öner, P.; -, al; Kato, F.; Noguchi, H.; Mardiana, L.; P Wardoyo, A. Y.; Dharmawan, H. A. *J. Phys. Conf. Ser.* **2022**, *2165*, 012014. [Crossref]

[97] Kusuma, K. B.; Manju, M.; Ravikumar, C. R.; Raghavendra, N.; Amulya, M. A. S.; Nagaswarupa, H. P.; Murthy, H. C. A.; Kumar, M. R. A.; Shashi Shekhar, T. R. *Appl. Surf. Sci. Adv.* **2022**, *11*, 100304. [Crossref]

[98] Panahi, A.; Monsef, R.; Imran, M. K.; Mahdi, A. A.; Kadhim Ruhaima, A. A.; Salavati-Niasari, M. *Int. J. Hydrogen Energy* **2023**, *48*, 3916. [Crossref]

[99] Panahi, A.; Ghanbari, M.; Dawi, E. A.; Monsef, R.; Reidh Abass, R.; Aljeboree, A. M.; Salavati-Niasari, M. *Ultrason. Sonochem.* **2023**, *95*, 106362. [Crossref]

[100] Alsalme, A.; Hesham, M.; Soltan, A.; Mohammed, N. N.; Nejm, A. Q.; Messih, M. F. A.; Hussein, I. A.; Ahmed, M. A. *Mater. Adv.* **2024**, 7278. [Crossref]

[101] Alsalme, A.; Hassan, M. M.; Eltawil, M. A.; Amin, A. E.; Soltan, A.; Messih, M. F. A.; Ahmed, M. A. *Heliyon* **2024**, *10*, e31221. [Crossref]

[102] Mahanta, U.; Khandelwal, M.; Deshpande, A. S. *Appl. Surf. Sci.* **2022**, *576*, 151745. [Crossref]

[103] Arora, I.; Chawla, H.; Chandra, A.; Sagadevan, S.; Garg, S. *Inorg. Chem. Commun.* **2022**, *143*, 109700. [Crossref]

[104] Erfan, N. A.; Mahmoud, M. S.; Kim, H. Y.; Barakat, N. A. M. *Front. Chem.* **2023**, *11*, 1. [Crossref]

[105] Gustavsen, K. R.; Feng, T.; Huang, H.; Li, G.; Narkiewicz, U.; Wang, K. *Materials (Basel).* **2023**, *16*, 1. [Crossref]

[106] Lim, C.; An, H. R.; Ha, S.; Myeong, S.; Min, C. G.; Chung, H. J.; Son, B.; Kim, C. Y.; Park, J. I.; Kim, H.; Lee, H. U.; Lee, Y. S. *Appl. Surf. Sci.* **2023**, *638*. [Crossref]

[107] Yang, Y.; Sun, T.; Ma, F.; Huang, L. F.; Zeng, Z. *ACS Appl. Mater. Interfaces* **2021**, *13*, 3377. [Crossref]

[108] Rathi, V. H.; Jeice, A. R.; Jayakumar, K. *Appl. Surf. Sci. Adv.* **2023**, *18*, 1. [Crossref]

[109] Slimani, Y.; Almessiere, M. A.; Mohamed, M. J. S.; Hannachi, E.; Caliskan, S.; Akhtar, S.; Baykal, A.; Gondal, M. A. *Catalysts* **2023**, *13*, 668. [Crossref]

[110] Kamani, H.; Ashrafi, S. D.; Lima, E. C.; Panahi, A. H.; Nezhad, M. G.; Abdipour, H. *Desalin. Water Treat.* **2023**, *289*, 155. [Crossref]

[111] Liza, T. Z.; Tusher, M. M. H.; Anwar, F.; Monika, M. F.; Amin, K. F.; Asrafuzzaman, F. N. U. *Results Mater.* **2024**, *22*, 100559. [Crossref]

[112] Asrafuzzaman, F. N. U.; Amin, K. F.; Gafur, M. A.; Gulshan, F. *Results Mater.* **2023**, *17*, 100384. [Crossref]

[113] Fazil, M.; Ahmad, T. *Catalysts* **2023**, *13*, 93. [Crossref]

[114] Alkorbi, A. S.; Muhammad Asif Javed, H.; Hussain, S.; Latif, S.; Mahr, M. S.; Mustafa, M. S.; Alsaiari, R.; Alhemiary, N. A. *Opt. Mater. (Amst).* **2022**, *127*, 112259. [Crossref]

[115] Romanovska, N.; Manoryk, P.; Yaremov, P.; Byeda, O.; Pershina, K.; Kazdobin, K. *Mater. Today Proc.* **2022**, *50*, 435. [Crossref]

[116] Ghanbarnezhad, M.; Parvareh, A.; Keshavarz Moraveji, M.; Jorfi, S. *J. Photochem. Photobiol. A Chem.* **2022**, *431*, 114044. [Crossref]

[117] Kodan, N.; Kumar, R.; Bai, R.; Mehta, B. R. *Renew. Energy* **2024**, *237*, 121734. [Crossref]

[118] Martín-Camacho, U. J.; Torres-Ramos, M. I.; González-Vargas, O. A.; Sánchez-Burgos, J. A.; Pérez-Larios, A. *Mater. Lett.* **2024**, *366*, 136528. [Crossref]

[119] Rosario, A. V.; Pereira, E. C. *Appl. Catal. B Environ.* **2014**, *144*, 840. [Crossref]

[120] Zhang, L.; Ran, J.; Qiao, S.-Z.; Jaroniec, M. *Chem. Soc. Rev.* **2019**, *48*, 5184. [Crossref]

[121] Khatun, M.; Mitra, P.; Mukherjee, S. *Hybrid Adv.* **2023**, *4*, 100079. [Crossref]

[122] El-Kalliny, A. S.; Abdel-Wahed, M. S.; El-Zahhar, A. A.; Hamza, I. A.; Gad-Allah, T. A. *Discov. Nano* **2023**, *18*, 68. [Crossref]

[123] Andrei A. Bunaciu, E. gabriela U.; Hassan Y. A.-E. *Crit. Rev. Anal. Chem.* **2015**, *45*, 289.

[124] Paranthaman, R.; Moses, J. A.; Anandharamakrishnan, C. *Food Anal. Methods* **2021**, *14*, 1054. [Crossref]

[125] Hassanzadeh-Tabrizi, S. A. *J. Alloys Compd.* **2023**, *968*, 171914. [Crossref]

[126] Iqbal, M. J.; Yaqub, N.; Sepiol, B.; Ismail, B. *Mater. Res. Bull.* **2011**, *46*, 1837. [Crossref]

[127] Majumdar, S. *Ceram. Int.* **2015**, *41*, 14350. [Crossref]

[128] Rahmani, K.; G. H., M.; and Atrian, A. *Powder Metall.* **2018**, *61*, 164. [Crossref]

[129] Delhez, R.; de Keijser, T. H.; Mittemeijer, E. J. *Fresenius'*

Zeitschrift für Anal. Chemie **1982**, *312*, 1. [Crossref]

[130] Masoumi, M.; Rahmati, S.; Saraiva, B. R. C.; Marçal, L. A. B.; Béreš, M.; de Abreu, H. F. G. *Mater. Sci. Eng. A* **2024**, *897*, 146363. [Crossref]

[131] Hu, Y.; Pan, Y.; Wang, Z.; Lin, T.; Gao, Y.; Luo, B.; Hu, H.; Fan, F.; Liu, G.; Wang, L. *Nat. Commun.* **2020**, *11*, 1. [Crossref]

[132] Lazaro, S. de; Penteado, R. F.; Tebcherani, S. M.; Berger, D.; Varela, J. A.; Kubaski, E. T. *Quim. Nova* **2012**, *35*, 920. [Crossref]

[133] Wen, W.; Hai, J.; Yao, J.; Gu, Y.-J.; Kobayashi, H.; Tian, H.; Sun, T.; Chen, Q.; Yang, P.; Geng, C.; Wu, J.-M. *Chem. Mater.* **2021**, *33*, 1489. [Crossref]

[134] Qi, W. H.; Wang, M. P.; Su, Y. C. *J. Mater. Sci. Lett.* **2002**, *21*, 877. [Crossref]

[135] French, A. D. *Cellulose* **2020**, *27*, 5445. [Crossref]

[136] Tarani; Arvanitidis, I.; Christofilos, D.; Bikiaris, D. N.; Chrissafis, K.; Vourlias, G. *J. Mater. Sci.* **2023**, *58*, 1621. [Crossref]

[137] Smith, S. J.; Stevens, R.; Liu, S.; Li, G.; Navrotsky, A.; Boerio-Goates, J.; Woodfield, B. F. *Am. Mineral.* **2009**, *94*, 236. [Crossref]

[138] Zhang, M.; Chen, T.; Wang, Y. *RSC Adv.* **2017**, *7*, 52755. [Crossref]

[139] Shah, A. H.; Rather, M. A. *ChemistrySelect* **2021**, *6*, 987. [Crossref]

[140] Serga, V.; Burve, R.; Krumina, A.; Romanova, M.; Kotomin, E. A.; Popov, A. I. *Crystals* **2021**, *11*, 431. [Crossref]

[141] Shah, A. H.; Rather, M. A. *Mater. Today Proc.* **2021**, *44*, 482. [Crossref]

[142] Wojciechowska, A.; Markowska-Szczupak, A.; Lendzion-Bieluń, Z. *Materials* **2022**, *15*, 1863. [Crossref]

[143] Babyszko, A.; Wanag, A.; Sadłowski, M.; Kusiak-Nejman, E.; Morawski, A. W. *Catalysts* **2022**, *12*, 1372. [Crossref]

[144] Napruszewska, B. D.; Walczyk, A.; Duraczyńska, D.; Kryściak-Czerwenka, J.; Karcz, R.; Gaweł, A.; Nowak, P.; Serwicka, E. M. *Nanomaterials* **2024**, *14*, 1130. [Crossref]

[145] Žener, B.; Matoh, L.; Reli, M.; Škapin, A. S.; Korošec, R. C. *Acta Chim. Slov.* **2022**, *69*, 217. [Crossref]

[146] Dontsova, T.; Kyrii, S.; Yanushevska, O.; Suprunchuk, V.; Kosogina, I. *Chem. Pap.* **2022**, *76*, 7667. [Crossref]

[147] Kusior, A.; Jeleń, P.; Sitarz, M.; Świerczek, K.; Radecka, M. *Catalysts* **2023**, *13*, 671. [Crossref]

[148] Irwansyah, F. S.; Amal, A. I.; Diyanthi, E. W.; Hadisantoso, E. P.; Noviyanti, A. R.; Eddy, D. R.; Risdiana, R. *ASEAN J. Sci. Eng.* **2024**, *4*, 61. [Crossref]

[149] Osterrieth, J. W. M.; Rampersad, J.; Madden, D.; Rampal, N.; Skoric, L.; Connolly, B.; Allendorf, M. D.; Stavila, V.; Snider, J. L.; Ameloot, R.; Marreiros, J.; Ania, C.; Azevedo, D.; Vilarrasa-Garcia, E.; Santos, B. F.; Bu, X. H.; Chang, Z.; Bunzen, H.; Champness, N. R.; Griffin, S. L.; Chen, B.; Lin, R. B.; Coasne, B.; Cohen, S.; Moreton, J. C.; Colón, Y. J.; Chen, L.; Clowes, R.; Coudert, F. X.; Cui, Y.; Hou, B.; D'Alessandro, D. M.; Doheny, P. W.; Dincă, M.; Sun, C.; Doonan, C.; Huxley, M. T.; Evans, J. D.; Falcaro, P.; Ricco, R.; Farha, O.; Idrees, K. B.; Islamoglu, T.; Feng, P.; Yang, H.; Forgan, R. S.; Bara, D.; Furukawa, S.; Sanchez, E.; Gascon, J.; Telalović, S.; Ghosh, S. K.; Mukherjee, S.; Hill, M. R.; Sadiq, M. M.; Horcajada, P.; Salcedo-Abraira, P.; Kaneko, K.; Kukobat, R.; Kenvin, J.; Keskin, S.; Kitagawa, S.; Otake, K. ichi; Lively, R. P.; DeWitt, S. J. A.; Llewellyn, P.; Lotsch, B. V.; Emmerling, S. T.; Pütz, A. M.; Martí-Gastaldo, C.; Padial, N. M.; García-Martínez, J.; Linares, N.; Maspoch, D.; Suárez del Pino, J. A.; Moghadam, P.; Oktavian, R.; Morris, R. E.; Wheatley, P. S.; Navarro, J.; Petit, C.; Danaci, D.; Rosseinsky, M. J.; Katsoulidis, A. P.; Schröder, M.; Han, X.; Yang, S.; Serre, C.; Mouchaham, G.; Sholl, D. S.; Thyagarajan, R.; Siderius, D.; Snurr, R. Q.; Goncalves, R. B.; Telfer, S.; Lee, S. J.; Ting, V. P.; Rowlandson, J. L.; Uemura, T.; Iiyuka, T.; van der Veen, M. A.; Rega, D.; Van Speybroeck, V.; Rogge, S. M. J.; Lamaire, A.; Walton, K. S.; Bingel, L. W.; Wuttke, S.; Andreo, J.; Yaghi, O.; Zhang, B.; Yavuz, C. T.; Nguyen, T. S.; Zamora, F.; Montoro, C.; Zhou, H.; Kirchon, A.; Fairen-Jimenez, D. *Adv. Mater.* **2022**, *34*. [Crossref]

[150] Maziarka, P.; Wurzer, C.; Arauzo, P. J.; Dieguez-Alonso, A.; Mašek, O.; Ronsse, F. *Chem. Eng. J.* **2021**, *418*, 129234. [Crossref]

[151] Bisht, G. S.; Singh, A. *J. Clust. Sci.* **2024**, *35*, 3095. [Crossref]

[152] Rahmiati, T.; Chen, C.-C.; Saad, A.; Setijogiarto, N. E.; Apriana, A. *Recent Eng. Sci. Technol.* **2023**, *01*, 1.

[153] Jalawkhan, R. S.; Ouda, A. A.; Abdul-Lettif, A. M.; Mohamad Alosfur, F. K. *IOP Conf. Ser. Mater. Sci. Eng.* **2020**, *928*, 072159. [Crossref]

[154] Thammaacheep, P.; Suriwong, T.; Jannoey, P.; Nakaruk, A.; Channei, D. *Green Chem. Lett. Rev.* **2024**, *17*, 2433607. [Crossref]

[155] Asadzadeh Patehkhor, H.; Fattahi, M.; Khosravi-Nikou, M. *Sci. Rep.* **2021**, *11*, 24177. [Crossref]

[156] Okoli, C. S.; Okonkwo, P. C.; Abdul, B. **2024**, *14*, 30. [Crossref]

[157] Nga, N. K.; Mai, N. T. T. *Vietnam J. Chem.* **2024**, *62*, 827. [Crossref]

[158] Yitagesu, G. B.; Leku, D. T.; Seyume, A. M.; Workneh, G. A. *ACS Omega* **2024**, *9*, 41301. [Crossref]

[159] Rosdiana, E. A.; Prasetya, N. B. A.; Gunawan, G. *Trends Sci.* **2023**, *20*, 6670. [Crossref]

[160] An, H.-R.; Lim, C.; Min, C. G.; Son, B.; Kim, C.-Y.; Park, J.-I.; Kim, J. P.; Jeong, Y.; Seo, J.; Lee, M.; Park, J.; Lee, Y.-S.; Lee, H. U. *Chemosphere* **2024**, *355*, 141859. [Crossref]

[161] Barkouch, H.; Bessbousse, H.; Amar, M.; Bouzzine, S. M.; Hamidi, M.; El Mhammedi, M. A.; Alaoui, O. T. *Opt. Mater. (Amst).* **2023**, *146*, 114507. [Crossref]

[162] Pietro; Ballarin, B.; Arcozzi, S.; Brattich, E.; Lucarelli, F.; Nava, S.; Gómez-Cascales, P. J.; Orza, J. A. G.; Tositti, L. *Atmos. Environ.* **2021**, *252*, 118297. [Crossref]

[163] Li, C. M.; Zhang, S.; Chen, H.; Ye, W. *J. Appl. Phys.* **2023**, *133*, 95104. [Crossref]

[164] Honson, V.; Huynh-Thu, Q.; Arnison, M.; Monaghan, D.; Isherwood, Z. J.; Kim, J. *Front. Psychol.* **2020**, *11*, 1. [Crossref]

[165] Morales-Mendoza, J. E.; Paraguay-Delgado, F. *Mater. Lett.* **2021**, *291*, 129494. [Crossref]

[166] Cai, Y.; Kiyokawa, H.; Nagai, T.; Haghzare, L.; Arnison, M.; Kim, J. *J. Opt. Soc. Am. A* **2023**, *40*, A220. [Crossref]

[167] Landi, S.; Segundo, I. R.; Freitas, E.; Vasilevskiy, M.; Carneiro, J.; Tavares, C. J. *Solid State Commun.* **2022**, *341*, 114573. [Crossref]

[168] Sundararajan, M.; Sukumar, M.; Dash, C. S.; Sutha, A.; Suresh, S.; Ubaidullah, M.; Al-Enizi, A. M.; Raza, M. K.; Kumar, D. *Phys. B Condens. Matter* **2022**, *644*, 414232. [Crossref]

[169] Klein, J.; Kampermann, L.; Mockenhaupt, B.; Behrens, M.; Strunk, J.; Bacher, G. *Adv. Funct. Mater.* **2023**, *33*, 1. [Crossref]

[170] Nawaz, A.; Khan, A.; Ali, N.; Mao, P.; Gao, X.; Ali, N.; Bilal, M.; Khan, H. *Chemosphere* **2022**, *289*, 133121. [Crossref]

[171] Jubu, P. R.; Obaseki, O. S.; Ajayi, D. I.; Danladi, E.; Chahrour, K. M.; Muhammad, A.; Landi, S.; Igbawua, T.; Chahul, H. F.; Yam, F. K. *J. Opt.* **2024**, 1. [Crossref]

[172] Jasim, A.; Salman, O. *J. Appl. Sci. Nanotechnol.* **2023**, *3*, 59. [Crossref]

[173] Utami, M.; Wang, S.; Fajarwati, F. I.; Salsabilla, S. N.; Dewi, T. A.; Fitri, M. *Crystals* **2023**, *13*, 588. [Crossref]

[174] Nong, L. X.; Nguyen, V. H.; Lee, T.; Bach, L. G.; Nguyen, T. D. *Chem. Eng. Technol.* **2023**, *46*, 2532. [Crossref]

[175] Asaad Mahdi, M.; Farhan, M. A.; Mahmoud, Z. H.; Mahdi Rheima, A.; sabri Abbas, Z.; Kadhim, M. M.; dhari jawad al-bayati, A.; Salam Jaber, A.; Hachim, S. K.; Hussain Ismail, A. *Arab. J. Chem.* **2023**, *16*, 104992. [Crossref]

[176] Tuo, B.; Wang, S.; Xiang, H.; Wang, J.; Mo, Y. *Desalin. Water Treat.* **2024**, *318*, 100328. [Crossref]

[177] Ratshiedana, R.; Mafa, P. J.; Fakayode, O. J.; Mishra, A. K.; Kuvarega, A. T. *Opt. Mater. (Amst).* **2024**, *157*, 116125. [Crossref]

[178] Shani, B.; Liccardo, L.; Bordin, M.; Martín, I. B.; Infantes-Molina, A.; Rodríguez-Castellón, E.; Ibrahim, K. B.; Vomiero, A.; Moretti, E. *Adv. Sustain. Syst.* **2024**, *2400375*, 1. [Crossref]

[179] Kacem, K.; Casanova-Chafer, J.; Hamrouni, A.; Ameur, S.; Güell, F.; Nsib, M. F.; Llobet, E. *Bull. Mater. Sci.* **2023**, *46*, 83. [Crossref]

[180] Fahim, S. A.; Zahan, N.; Shathy, R. A.; Quddus, M. S.; Moniruzzaman, M.; Masum, S. M.; Molla, M. A. I. *Mater. Chem. Phys.* **2023**, *305*, 127937. [Crossref]

[181] Yadav, V.; Sharma, H.; Singh, R. K.; Kumar, A.; Saini, V. K. *Appl. Nanosci.* **2023**, *13*, 5903. [Crossref]

[182] Widiyandari, H.; Nashir, M.; Parasdila, H.; Almas, K. F.; Suryana, R. *Bull. Chem. React. Eng. Catal.* **2023**, *18*, 593. [Crossref]

[183]

[184] Zhou, W., Apkarian, R., Wang, Z.L., Joy, D. Fundamentals of Scanning Electron Microscopy (SEM). In: Zhou, W., Wang, Z.L. (eds) Scanning Microscopy for Nanotechnology. Springer, New York, NY, 2006. [Crossref]

[185] Mohammed, A.; Abdullah, A. *Proc. 2018 Int. Conf. Hydraul. Pneum. - HERVEX* **2018**, 77.

[186] Newbury, D. E.; Ritchie, N. W. M. *Scanning* **2013**, *35*, 141. [Crossref]

[187] Khalil, A. M.; El-Sayed, S. M.; Youssef, A. M. *Biomass Convers. Biorefinery* **2023**, 0123456789. [Crossref]

[188] Jain, A.; Kumar, M. *Small* **2024**, *20*, 2309100. [Crossref]

[189] Luo, W.; Blanchard, J.; Tonelli, D.; Taleb, A. *Micromachines* **2023**, *14*, 243. [Crossref]

[190] Tahmasebi, E.; Mohammadi, M.; Yazdanian, M.; Alam, M.; Abbasi, K.; Hosseini, H. M.; Tavakolizadeh, M.; Khayatan, D.; Hassani, Z.; Tebyaniyan, H. *J. Basic Microbiol.* **2023**, *63*, 1030. [Crossref]

[191] Kočí, K.; Obalová, L.; Matějová, L.; Plachá, D.; Lacný, Z.; Jirkovský, J.; Šolcová, O. *Appl. Catal. B Environ.* **2009**, *89*, 494. [Crossref]

[192] Saka, A.; Jule, L. T.; Badassa, B.; Gudata, L.; Nagaprasad, N.; Shanmugam, R.; Dwarampudi, L. P.; Seenivasan, V.; Ramaswamy, K. *BMC Chem.* **2024**, *18*, 123. [Crossref]

[193] Li, P.; Huang, Y.; Zhang, Y.; Chen, L. *Chem. Eng. J.* **2024**, *479*, 147829. [Crossref]

[194] Montazerghaem, L.; Keramatifarhodbonab, M.; Naeimi, A. *Heliyon* **2024**, *10*, e24789. [Crossref]

[195] Alimard, P.; Gong, C.; Itskou, I.; Kafizas, A. *Chemosphere* **2024**, *368*, 143728. [Crossref]

[196] Mazouzi, D. E.; Djani, F.; Soukeur, A.; Bouchal, W.; Manseri, A.; Derkaoui, K.; Martínez-Arias, A.; Ksouri, A.; Şen, F.; Kaci, M. M. *Surfaces and Interfaces* **2024**, *44*, 103581. [Crossref]

[197] Wang, X.; Liu, B.; Ma, S.; Zhang, Y.; Wang, L.; Zhu, G.; Huang, W.; Wang, S. *Nat. Commun.* **2024**, *15*, 2600. [Crossref]

[198] Bissenova, M.; Umirzakov, A.; Mit, K.; Mereke, A.; Yerubayev, Y.; Serik, A.; Kuspanov, Z. *Molecules* **2024**, *29*, 1101. [Crossref]

[199] Raeisipour, J.; Salari, D.; Niaei, A.; Hosseini, S. A.; Maleki, A. *Ceram. Int.* **2024**, *50*, 18125. [Crossref]

[200] Kadam, V.; Jagtap, C.; Kumkale, V.; Rednam, U.; Lokh, P.; Pathan, H. *Engineered Science* **2024**, *28*, 1077. [Crossref]

[201] Alam, M. A.; Bishwas, R. K.; Mostofa, S.; Jahan, S. A. *South African J. Chem. Eng.* **2024**, *49*, 73. [Crossref]

[202] Schutte-Smith, M.; Erasmus, E.; Mogale, R.; Marogoa, N.; Jayiya, A.; Visser, H. G. *J. Coatings Technol. Res.* **2023**, *20*, 789. [Crossref]

[203] Thakur, N.; Thakur, N.; Kumar, A.; Thakur, V. K.; Kalia, S.; Arya, V.; Kumar, A.; Kumar, S.; Kyzas, G. Z. *Sci. Total Environ.* **2024**, *914*, 169815. [Crossref]

[204] Mei, J.; Gao, X.; Zou, J.; Pang, F. *Catalysts* **2023**, *13*, 974. [Crossref]

[205] Wang, X.; Wang, F.; Sang, Y.; Liu, H. *Adv. Energy Mater.* **2017**, *7*, 1700473. [Crossref]

[206] Samarasinghe, L. V.; Muthukumaran, S.; Baskaran, K. *Chemosphere* **2024**, *349*, 140818. [Crossref]

[207] Chanchal Hazra. *Sci. Dialectica* **2024**, *1*. [Crossref]

[208] Jo, W.-K.; Tayade, R. J. *Ind. Eng. Chem. Res.* **2014**, *53*, 2073. [Crossref]

[209] Li, C.; Lu, Z.; Ao, X.; Sun, W.; Huang, X. *Chem. Eng. J.* **2022**, *427*, 130828. [Crossref]

[210] Herrera-Muñoz, J.; Cabrera-Reina, A.; Salazar-González, R.; Miralles-Cuevas, S. *J. Environ. Chem. Eng.* **2024**, *12*, 112471. [Crossref]

[211] Das, A. *Lett. Org. Chem.* **2022**, *19*, 283. [Crossref]

[212] Sheldon, R. A.; Brady, D. *ChemSusChem* **2022**, *15*, e202102628. [Crossref]

[213] Rohmatullaili; Ahmad, N.; Erviana, D.; Zultriana; Savira, D.; Mohadi, R.; Lesbani, A. *Inorg. Chem. Commun.* **2024**, *161*, 112101. [Crossref]

[214] Hsu, T.-C.; Teng, Y.-T.; Yeh, Y.-W.; Fan, X.; Chu, K.-H.; Lin, S.-H.; Yeh, K.-K.; Lee, P.-T.; Lin, Y.; Chen, Z.; Wu, T.; Kuo, H.-C. *Photonics* **2021**, *8*. 196. [Crossref]

[215] Bertagna Silva, D.; Buttiglieri, G.; Babić, S. *Environ. Sci. Pollut. Res.* **2021**, *28*, 103. [Crossref]

[216] Fu, R.; Song, H.; Liu, X.; Zhang, Y.; Xiao, G.; Zou, B.; Waterhouse, G. I. N.; Lu, S. *Chinese J. Chem.* **2023**, *41*, 1007. [Crossref]

[217] Chaudhary, G.; Dhwaj, A.; Verma, A.; Kumari, P.; Lal, K.; Verma, D.; Prabhakar, A. *ACS Omega* **2024**, *9*, 42267. [Crossref]

[218] Castro, G. G.; Pinto, P. A.; Favoreto, M. W.; Reis, A.; Viviana-Mora, M.; de Miranda, R. de C. M.; Cardenas, A. F. M.; Loguercio, A. D.; Tavarez, R. R. de J. *Photodiagnosis Photodyn. Ther.* **2024**, *50*, 104410. [Crossref]

[219] Pech, J.; Kunz, H.-C.; Martin, A.; Seidler, T.; Reich, F. *J. Food Meas. Charact.* **2025**, *19*, 1828. [Crossref]

[220] Kubiak, A. *Sci. Rep.* **2024**, *14*, 20563. [Crossref]

[221] Moral-Rodríguez, A. I.; Ramírez-Valencia, L. D.; Bailón-García, E.; Carrasco-Marín, F.; Pérez-Cadenas, A. F. *Environ. Res.* **2024**, *247*, 118120. [Crossref]

[222] Thangamuniyandi, P.; Umapathy, D.; Nagarajan, L.; Velanganni Arockiam, A. J. *Heliyon* **2025**, *11*, e41061. [Crossref]

[223] Zulfa, L. L.; Hidayat, A. R. P.; Utomo, W. P.; Subagyo, R.; Kusumawati, E. N.; Kusumawati, Y.; Hartanto, D.; Widyastuti, W.; Ediati, R. *Case Stud. Chem. Environ. Eng.* **2024**, *10*, 100828. [Crossref]

[224] Meky, A. I.; Hassaan, M. A.; Fetouh, H. A.; Ismail, A. M.; El Nemr, A. *Sci. Rep.* **2024**, *14*, 2016. [Crossref]

[225] Barquín, C.; Rivero, M. J.; Ortiz, I. *Chemosphere* **2024**, *349*, 140806. [Crossref]

[226] Gadore, V.; Singh, A. K.; Mishra, S. R.; Ahmaruzzaman, M. *Sci. Rep.* **2024**, *14*, 1118. [Crossref]

[227] Yazdanbakhsh, A.; Eslami, A.; Massoudinejad, M.; Gholami, Z.; Sarafraz, M.; Noorimotlagh, Z.; Adiban, M.; Mirzaee, S. A. *Sci. Rep.* **2024**, *14*, 29583. [Crossref]

[228] Kubiak, A. *Sci. Rep.* **2024**, *14*, 13827. [Crossref]

[229] Jamil, Q.; Žener, B.; Putar, U.; Matoh, L. *Heliyon* **2024**, *10*, e40019. [Crossref]

[230] Ahmad, I.; Ben Ahmed, S.; Shabir, M.; Imran, M.; Hassan, A. M.; Alatawi, N. S. *J. Ind. Eng. Chem.* **2024**, *130*, 105. [Crossref]

[231] Ribeiro, R.; Fanzeres, B. *Energy AI* **2024**, *15*, 100320. [Crossref]

[232] Sun, X.; Jiang, S.; Huang, H.; Li, H.; Jia, B.; Ma, T. *Angew. Chemie Int. Ed.* **2022**, *61*, e202204880. [Crossref]

[233] Balogh, T. S.; Velasco, M. V. R.; Pedriali, C. A.; Kaneko, T. M.; Baby, A. R. *An. Bras. Dermatol.* **2011**, *86*, 732.

[234] Wang, J.; Peng, Z.; Huang, J.; Zhang, Y.; Zhang, X.; Wang, Y.; Fu, Y.; Li, W.; Chen, J.; Chen, K. *Sol. Energy Mater. Sol. Cells* **2023**, *257*, 112348. [Crossref]

[235] Al-Baitai, A. Y.; Mahmood, M.; abdulhussein, S. F.; Abdalhadi, S. M. *Nanochemistry Res.* **2024**, *9*, 207. [Crossref]

[236] Ma, X.; Wang, L.; She, H.; Zhou, Y.; Wang, L.; Huang, J.; Wang, Q. *Front. Chem. Sci. Eng.* **2024**, *18*, 105. [Crossref]

[237] Pesqueira, J. F. J. R.; Pereira, M. F. R.; Silva, A. M. T. *J. Clean. Prod.* **2024**, *444*, 140845. [Crossref]

[238] González-Pereyra, D.; González-Rodríguez, L. M.; Villanueva-Rodríguez, M.; Alonso-Segura, D.; Aba-Guevara, C. G.; Sanjuan-Galindo, R.; Ramos-Delgado, N. A. *Top. Catal.* **2022**, *65*, 1062. [Crossref]

[239] Fdez-Sanromán, A.; Pazos, M.; Rosales, E.; Sanromán, A. *Catalysts* **2024**, *14*, 175. [Crossref]

[240] Chaudhuri, A.; Zondag, S. D. A.; Schuurmans, J. H. A.; van der Schaaf, J.; Noël, T. *Org. Process Res. Dev.* **2022**, *26*, 1279. [Crossref]

[241] Araújo, D. dos S.; Diniz, V. C. de S.; Torquato, R. A.; Costa, A. C. F. de M.; Moma, J.; Baloyi, J. In *Photocatalysts - Applications and Attributes*; IntechOpen, 2018. Vol. 23, pp 37–56. [Crossref]

[242] Gualda-Alonso, E.; Pichel, N.; Soriano-Molina, P.; Olivares-Ligero, E.; Cadena-Aponte, F. X.; Agüera, A.; Sánchez Pérez, J. A.; Casas López, J. L. J. *Hazard. Mater.* **2023**, *459*, 132101. [Crossref]

[243] Madadi Avargani, V.; Zendehboudi, S.; Osfouri, S.; Rostami, A. *J. Clean. Prod.* **2023**, *421*, 138240. [Crossref]

[244] Dufner, L.; Aresté-Saló, L.; Graells, M.; Pérez-Moya, M.; Kern, F.; Rheinheimer, W. *Open Ceram.* **2024**, *18*, 100599. [Crossref]

[245] Assadi, A. A.; Bouzaza, A.; Vallet, C.; Wolbert, D. *Chem. Eng. J.* **2014**, *254*, 124. [Crossref]

[246] Samy, M.; Tang, S.; Zhang, Y.; Leung, D. Y. C. *J. Environ. Manage.* **2024**, *370*, 122402. [Crossref]

[247] Madadi Avargani, V.; Zendehboudi, S.; Osfouri, S.; Rostami, A. *J. Clean. Prod.* **2023**, *421*, 138240. [Crossref]

[248] Ali, N. S.; Kalash, K. R.; Ahmed, A. N.; Albayati, T. M. *Sci. Rep.* **2022**, *12*, 16782. [Crossref]

[249] Hemanathan, G.; Karthikeyan, S.; Kathirvel, R. *Desalin. Water Treat.* **2024**, *320*, 100675. [Crossref]

[250] Tejashwini, D. M.; Harini, H. V; Nagaswarupa, H. P.; Naik, R.; Harlapur, S.; Basavaraju, N. *Results Chem.* **2024**, *7*, 101247. [Crossref]

[251] Kumari, H.; Sonia; Suman; Ranga, R.; Chahal, S.; Devi, S.; Sharma, S.; Kumar, S.; Kumar, P.; Kumar, S.; Kumar, A.; Parmar, R. *Water, Air, Soil Pollut.* **2023**, *234*, 349. [Crossref]

[252] Kurniawan, T. A.; Othman, M. H. D. In *Elsevier Series on Advanced Ceramic Materials*; Othman, M. H. D., Rahman, M. A., Matsuura, T., Adam, M. R., Mohd Makhtar, S. N. N. B. T.-A. C. for P. M., Eds.; Elsevier, 2024; pp 501–512. [Crossref]

[253] Iyyappan, J.; Gaddala, B.; Gnanasekaran, R.; Gopinath, M.; Yuvaraj, D.; Kumar, V. *Case Stud. Chem. Environ. Eng.* **2024**, *9*, 100599. [Crossref]

[254] Joseph, A.; Vijayanandan, A. *Inorganica Chim. Acta* **2023**, *545*, 121284. [Crossref]

[255] Yang, H.; Chen, J. *J. Environ. Chem. Eng.* **2024**, *12*, 112765. [Crossref]

[256] Castro-Rojas, J.; Rao, M. A.; Berruti, I.; Mora, M. L.; Garrido-Ramírez, E.; Polo-López, M. I. *Chem. Eng. J.*

2025, *503*, 157894. [Crossref]

[257] Bogatu, C.; Covei, M.; Polo-López, M. I.; Duta, A.; Malato, S. *Catal. Today* **2023**, *413–415*, 113947. [Crossref]

[258] Rodrigues-Silva, F.; V. M. Starling, M. C.; Amorim, C. C. *Sci. Total Environ.* **2022**, *850*, 157940. [Crossref]

[259] Ahtasham Iqbal, M.; Akram, S.; khalid, S.; Lal, B.; Hassan, S. U.; Ashraf, R.; Kezembayeva, G.; Mushtaq, M.; Chinibayeva, N.; Hosseini-Bandegharaei, A. *Environ. Res.* **2024**, *253*, 118947. [Crossref]

[260] Muscetta, M.; Ganguly, P.; Clarizia, L. *J. Environ. Chem. Eng.* **2024**, *12*, 113073. [Crossref]

[261] Majumder, A.; Otter, P.; Röher, D.; Bhatnagar, A.; Khalil, N.; Gupta, A. K.; Bresciani, R.; Arias, C. A. *J. Environ. Manage.* **2024**, *351*, 119672. [Crossref]

[262] Chauhan, P. S.; Singh, K.; Choudhary, A.; Brighu, U.; Singh, S. K.; Bhattacharya, S. *npj Clean Water* **2024**, *7*, 15. [Crossref]

[263] Ma, X.; Chen, X.; Yang, Y.; Zhang, C.; Zhang, F.; Chen, D.; Sharma, V. K.; Wang, J. *J. Environ. Chem. Eng.* **2024**, *12*, 111596. [Crossref]

[264] Khan, M. U. A.; Masood, H. M.; Ali, N.; Ashraf, M. *J. Chem. Soc. Pakistan* **2024**, *46*, 192. [Crossref]

[265] Wagdy, R.; Mubarak, M. F.; Mohamed, R. S.; El Shahawy, A. *RSC Adv.* **2024**, *14*, 10776. [Crossref]

[266] Aibuedefe, A. F.; Tina, A. E. *Sustain. Chem. Environ.* **2024**, *5*, 100076. [Crossref]

[267] Yuceturk, G. D. *Braz. J. Poult. Sci.* **2024**, *26, 001*. [Crossref]

[268] Al-Tameemi, H. M.; Sukkar, K. A.; Abbar, A. H.; Kuraimid, Z. K. *Case Stud. Chem. Environ. Eng.* **2024**, *9*, 100687. [Crossref]

[269] Constantin, M. A.; Constantin, L. A.; Ionescu, I. A.; Nicolescu, C. M.; Bumbac, M.; Tiron, O. *Processes* **2024**, *12*, 617. [Crossref]

[270] Rapti, I.; Kourkouta, T.; Malisova, E.-M.; Albanis, T.; Konstantinou, I. *Molecules* **2023**, *28*, 1170. [Crossref]

[271] Bhargava, N.; Bahadur, N.; Kansal, A. *J. Water Process Eng.* **2023**, *56*, 104302. [Crossref]

[272] Pandey, S.; Srivastava, A.; Rawat, P.; Chauhan, S. K.; Ram, A.; Diwedi, V. K.; Shukla, R. K.; Wadhwani, N. *ACS Omega* **2024**, *9*, 45169. [Crossref]

[273] Maniakova, G.; Rizzo, L. *J. Environ. Chem. Eng.* **2023**, *11*, 111356. [Crossref]

[274] Veras, T. B.; de Paiva, A. L. R.; Duarte, M. M. M. B.; Napoleão, D. C.; Cabral, J. J. S. P. *Chemosphere* **2019**, *222*, 961. [Crossref]

[275] Antonopoulou, M.; Evgenidou, E.; Lambropoulou, D.; Konstantinou, I. *Water Res.* **2014**, *53*, 215. [Crossref]

[276] Wei, Y.; Wu, Q.; Meng, H.; Zhang, Y.; Cao, C. *RSC Adv.* **2023**, *13*, 20584. [Crossref]

[277] Liu, Y.; Huang, J.; Guo, Z. *J. Environ. Chem. Eng.* **2024**, *12*, 113133. [Crossref]

[278] Alhmoud, S. H. *SSRG Int. J. Civ. Eng.* **2024**, *11*, 79. [Crossref]

[279] Chowdhury, A.; Mamatha, D.; Chakravarti, S.; Kumar, R. Prasad, M., Kumar, R., Ghosh, M., Syed, S. M., Chakravarti, S., Eds.; Springer Nature Singapore: Singapore, 2024, pp 363–377. [Crossref]

[280] Zhou, R.; O'Rourke, C.; Han, R.; Yusufu, D.; Mills, A. *J. Photochem. Photobiol. A Chem.* **2024**, *454*, 115677. [Crossref]

[281] Guo, B.; Tao, Y.; Yang, T.; Su, X.; Tan, X.; Tian, W.; Xie, L. *J. Mater. Chem. B* **2024**, *12*, 9459. [Crossref]

[282] Nomura, Y.; Hanada, N.; Liu, Y. *J. Univ. Shanghai Sci. Technol.* **2023**, *45*, 1. [Crossref]

[283] Tao, Y.-K.; Tseng, Y.-W.; Tzou, K.-Y.; Kuo, C.-Y.; Nguyen, H. T.; Lu, H.-T.; Chuang, A. E.-Y. *Int. J. Biol. Macromol.* **2024**, *276*, 133647. [Crossref]

[284] Ojo, S.; Tsai, Y. H.; Samia, A. C. S.; Yu, X. *Catalysts* **2024**, *14*, 783. [Crossref]

[285] Bakina, O.; Pikuschak, E.; Prokopchuk, A.; Evplonova, E.; Plaksina, T.; Avgustinovich, A.; Spirina, L.; Vorozhtsov, A.; Yakovlev, N.; Lerner, M. *Coatings* **2024**, *14*, 241. [Crossref]

[286] Dong, X.; Liu, Y.; Adcock, A. F.; Sheriff, K.; Liang, W.; Yang, L.; Sun, Y.-P. *Int. J. Mol. Sci.* **2024**, *25*, 2196. [Crossref]

[287] Feng, J.; Zhang, K.; Huang, S.; Zhang, J.; Huo, B.; Cao, X.; Cong, P. *Glob. Nest J.* **2024**, *26*, 1. [Crossref]

[288] Aygun, A.; Tiri, R. N. E.; Bayat, R.; Sen, F. *J. Hazard. Mater. Adv.* **2024**, *16*, 100464. [Crossref]

[289] Ha, O.-Y.; Oh, J.-M.; Kim, S. *Chem. Eng. J.* **2024**, *496*, 153851. [Crossref]

[290] Behzadnia, A.; Montazer, M.; Mahmoudi Rad, M.; Rastgoo, M. *Heliyon* **2024**, *10*, e36522. [Crossref]

[291] Yen, L.-T.; Weng, C.-H.; Tzeng, J.-H.; Chen, Y.-C.; Jacobson, A. R.; Lin, Y.-T. *Sep. Purif. Technol.* **2024**, *345*, 127298. [Crossref]

[292] Vevers, R.; Kulkarni, A.; Seifert, A.; Pöschel, K.; Schlenstedt, K.; Meier-Haack, J.; Mezule, L. *Molecules* **2024**, *29*, 1274. [Crossref]

[293] Hsu, C. Y.; Mahmoud, Z. H.; Abdullaev, S.; Ali, F. K.; Ali Naeem, Y.; Mzahim Mizher, R.; Morad Karim, M.; Abdulwahid, A. S.; Ahmadi, Z.; Habibzadeh, S.; kianfar, E. *Case Stud. Chem. Environ. Eng.* **2024**, *9*, 100626. [Crossref]

[294] Wang, S.; Huang, Q.; Liu, X.; Li, Z.; Yang, H.; Lu, Z. *ACS Biomater. Sci. Eng.* **2019**, *5*, 2030. [Crossref]

[295] Seshadri, K.; Abad, A. N. D.; Nagasawa, K. K.; Yost, K. M.; Johnson, C. W.; Dror, M. J.; Tang, Y. *Chem. Rev.* **2025**, *125*, 3814. [Crossref]

[296] Appleby, M.V., Pritchard, D., Weinstein, J.A. Photocatalytic Processes for Water Treatment. In: Leal Filho, W., Azul, A.M., Brandli, L., Lange Salvia, A., Wall, T. (eds) Clean Water and Sanitation. Encyclopedia of the UN Sustainable Development Goals. Springer, Cham. 2022. [Crossref]

[297] Serov, D. A.; Gritsaeva, A. V.; Yanbaev, F. M.; Simakin, A. V.; Gudkov, S. V. *Int. J. Mol. Sci.* **2024**, *25*, 10519. [Crossref]

[298] Wu, B.; Wang, J.; He, X.; Dai, H.; Zheng, X.; Ma, J.; Yao, Y.; Liu, D.; Yu, W.; Chen, B.; Chu, C. *Environ. Sci. Technol.* **2024**, 58, 20181. [Crossref]

How to cite this article

França, Y. K. S.; Pereira, K. S.; Feitosa, Y. H. C.; Marques, V. B.; Souza, D. R. *Orbital: Electronic J. Chem*. **2025**, *17*, 355. DOI:

http://dx.doi.org/10.17807/orbital.v7i4.23400